



Characterization of the particle size distribution, mineralogy, and Fe mode of occurrence of dust-emitting sediments from the Mojave Desert, California, USA

Adolfo González-Romero^{1,2,3}, Cristina González-Flórez^{1,3}, Agnesh Panta⁴, Jesús Yus-Díez⁵, Patricia Córdoba², Andres Alastuey², Natalia Moreno², Melani Hernández-Chiriboga¹, Konrad Kandler⁴, Martina Klose⁶, Roger N. Clark⁷, Bethany L. Ehlmann⁸, Rebecca N. Greenberger⁸, Abigail M. Keebler⁸, Phil Brodrick⁹, Robert Green⁹, Paul Ginoux¹⁰, Xavier Querol², and Carlos Pérez García-Pando^{1,11}

¹Barcelona Supercomputing Center (BSC), Barcelona, Spain

²Institute of Environmental Assessment and Water Research (IDAEA-CSIC), Spanish Research Council, Barcelona, Spain

³Polytechnical University of Catalonia (UPC), Barcelona, Spain

⁴Institute of Applied Geosciences, Technical University Darmstadt, Darmstadt, Germany

⁵Centre for Atmospheric Research, University of Nova Gorica, Ajdovščina, Slovenia

⁶Institute of Meteorology and Climate Research Troposphere Research (IMKTRO), Karlsruhe Institute of Technology (KIT), Karlsruhe, Germany

⁷PSI Planetary Science Institute, Tucson, AZ, USA

⁸Division of Geological and Planetary Sciences, California Institute of Technology, Pasadena, CA, USA

⁹Jet Propulsion Laboratory, California Institute of Technology, Pasadena, CA, USA

¹⁰NOAA Geophysical Fluid Dynamics Laboratory, Princeton, NJ, USA

¹¹Catalan Institution for Research and Advanced Studies (ICREA), Barcelona, Spain

Correspondence: Adolfo González-Romero (agonzal3@bsc.es) and Xavier Querol (xavier.querol@idaea.csic.es)

Received: 14 February 2024 – Discussion started: 27 February 2024

Revised: 6 June 2024 – Accepted: 10 June 2024 – Published: 22 August 2024

Abstract. Constraining dust models to understand and quantify the effect of dust upon climate and ecosystems requires comprehensive analyses of the physiochemical properties of dust-emitting sediments in arid regions. Building upon previous studies in the Moroccan Sahara and Iceland, we analyse a diverse set of crusts and aeolian ripples ($n = 55$) from various potential dust-emitting basins within the Mojave Desert, California, USA. Our focus is on characterizing the particle size distribution (PSD), mineralogy, aggregation/cohesion state, and Fe mode of occurrence. Our results show differences in fully and minimally dispersed PSDs, with crusts exhibiting average median diameters of 92 and 37 μm , respectively, compared to aeolian ripples with 226 and 213 μm , respectively. Mineralogical analyses unveiled strong variations between crusts and ripples, with crusts being enriched in phyllosilicates (24 % vs. 7.8 %), carbonates (6.6 % vs. 1.1 %), Na salts (7.3 % vs. 1.1 %), and zeolites (1.2 % and 0.12 %) and ripples being enriched in feldspars (48 % vs. 37 %), quartz (32 % vs. 16 %), and gypsum (4.7 % vs. 3.1 %). The size fractions from crust sediments display a homogeneous mineralogy, whereas those of aeolian ripples display more heterogeneity, mostly due to different particle aggregation. Bulk Fe content analyses indicate higher concentrations in crusts (3.0 ± 1.3 wt %) compared to ripples (1.9 ± 1.1 wt %), with similar proportions in their Fe mode of occurrence: nano-sized Fe oxides and readily exchangeable Fe represent ~ 1.6 %, hematite and goethite ~ 15 %, magnetite/maghemite ~ 2.0 %, and structural Fe in silicates ~ 80 % of the total Fe. We identified segregation patterns in the PSD and mineralogy differences in Na salt content within

the Mojave basins, which can be explained by sediment transportation dynamics and precipitates due to ground-water table fluctuations described in previous studies in the region. Mojave Desert crusts show similarities with previously sampled crusts in the Moroccan Sahara in terms of the PSD and readily exchangeable Fe yet exhibit substantial differences in mineralogical composition, which should significantly influence the characteristic of the emitted dust particles.

1 Introduction

Desert dust produced by the wind erosion of arid and semi-arid surfaces has significant effects on climate, ecosystems, and health (Weaver et al., 2002; Goudie and Middleton, 2006; Sullivan et al., 2007; Crumeyrolle et al., 2008; De Longueville et al., 2010; Karanasiou et al., 2012; Pérez García-Pando et al., 2014; among others). Dust affects energy and water cycles through its absorption and scattering of both shortwave (SW) and longwave (LW) radiation (Perez et al., 2006; Miller et al., 2014) and exerts influence on cloud formation, precipitation patterns, and the associated indirect radiative forcing by serving as nuclei for liquid and ice clouds (e.g. Harrison et al., 2019). Dust also undergoes heterogeneous chemical reactions in the atmosphere that enhance particles' hygroscopicity and modify their optical properties (Bauer and Koch, 2005), and when deposited into ocean waters, its bioavailable iron content acts as a catalyst for photosynthesis by ocean phytoplankton, thereby increasing carbon dioxide uptake and influencing the global carbon cycle (Jickells et al., 2005). Dust primarily originates from arid inland basins, which include various sedimentary environments such as aeolian deposits, endorheic depressions, and fluvial- and alluvial-dominated systems (Bullard et al., 2011). Wind typically mobilizes loose sand from adjacent ripples or dunes, which then erodes more consolidated surfaces, typically paved sediments and crusts, to release dust (Stout and Lee, 2003; Shao et al., 2011). Atmospheric dust emission models have improved by identifying preferential dust sources using criteria like topography and hydrology (Ginoux et al., 2001). However, these models still struggle with capturing small-scale variability, partly due to the lack of relevant soil measurements in arid regions, despite advancements in understanding the geomorphological and sedimentological factors influencing dust emissions (Bullard et al., 2011). For instance, the particle size distribution (PSD) and cohesion of the sediments affect saltation bombardment and aggregate disintegration processes involved in dust emission (Shao et al., 1993).

Understanding the mineral composition of dust is also crucial for assessing its climate impact. Dust contains various minerals such as quartz, clay minerals, feldspars, carbonates, salts, and iron oxides. The climate effects of dust are influenced by these minerals' relative abundances, sizes, shapes, and mixing states. For example, iron oxides control solar radiation absorption by dust (Formenti et al., 2014; Engel-

brecht et al., 2016; Di Biagio et al., 2019; Zubko et al., 2019), nano-sized Fe oxides and easily exchangeable Fe increase the fertilizing effect of dust in ocean and terrestrial ecosystems (Hettiarachchi et al., 2019, 2020; Baldo et al., 2020), K-feldspar and quartz impact ice nucleation in clouds (Atkinson et al., 2013; Harrison et al., 2019; Chatziparaschos et al., 2023), and calcite influences acid reactions on dust surfaces (Paulot et al., 2016). The mineralogical composition of dust can vary significantly across different regions due to geological and climatic factors (Claquin et al., 1999; Journet et al., 2014). However, most models assume a globally uniform dust composition due to limited global data on parent soil sources. Only a few models account for dust mineralogical composition variations (e.g. Scanza et al., 2015; Perlwitz et al., 2015; Li et al., 2021; Gonçalves Ageitos et al., 2023; Obiso et al., 2024) using global soil type atlases that are based on the extrapolation of a limited number of soil analyses (Claquin et al., 1999; Journet et al., 2014). These atlases rely on assumptions about soil texture and colour and often base their data on soil samples taken from depths deeper than those relevant to wind erosion, and the method used to characterize particle size and associated mineralogy fully breaks down natural soil aggregates.

Since 2022, the EMIT mission has been acquiring comprehensive measurements of surface mineralogical composition for use in Earth system models (Green et al., 2020). EMIT employs imaging spectroscopy across the visible to short-wavelength infrared (VSWIR) spectral range from the International Space Station to map the occurrence and estimate the abundance of 10 key dust source minerals. Additionally, EMIT has the potential to estimate surface soil texture. While identifying dominant surface minerals has traditionally been a strength of spectrometers, quantifying these minerals poses significant challenges. Factors such as mineral grain size and composition can affect spectral absorptions, certain dominant materials like quartz and feldspar exhibit minimal absorption features, and the presence of other materials can further complicate the analysis.

Overall, there is a notable lack of comprehensive measurements characterizing relevant properties of surface sediments in dust source regions. This gap hampers our ability to evaluate and constrain mineral abundance derived from reflectance spectroscopy and to improve dust emission modelling. Addressing this issue, the FRontiers in dust mineraloGical coMposition and its Effects upoN climaTe (FRAGMENT) project has, over recent years, conducted a series

of coordinated and interdisciplinary field campaigns across remote dust source regions. The project's objectives include enhancing the understanding and quantification of dust source properties, examining their relationship with emitted dust characteristics, refining spaceborne spectroscopy retrievals of surface minerals (Green et al., 2020; Clark et al., 2024), and improving the representation of dust mineralogy in Earth system models (Perlwitz et al., 2015; Li et al., 2021; Gonçalves et al., 2023; Obiso et al., 2024). The FRAGMENT field campaigns involved regional sediment sampling in several regions and detailed wind erosion and dust emission measurements at selected sites. Studies stemming from these activities include those by González-Romero et al. (2023), González-Flórez et al. (2023), Panta et al. (2023), and González-Romero et al. (2024). These campaigns have been executed in various geographic locations, such as the Moroccan Sahara (2019), Iceland (2021), the Mojave Desert in the USA (2022), and Jordan (2022). Through these efforts, the FRAGMENT project contributes to filling critical knowledge gaps in dust source characterization.

Following our previous studies in the Moroccan Sahara (González-Romero et al., 2023) and Iceland (González-Romero et al., 2024), this study focuses on the characterization of dust-emitting sediments collected from the Mojave Desert in 2022. The Mojave Desert is a closed-basin wedge-shaped region located in the southwestern USA, between California and Nevada. The region is surrounded by mountain ranges and traversed by the Mojave River and other intermittent rivers for over 200 km from the San Bernardino Mountains to the east (Dibblee, 1967; Reheis et al., 2012). Despite its limited global importance (dust emission from North America represents only $\sim 3\%$ of global dust emission; Kok et al., 2021), the Mojave Desert is an important regional dust source (Ginoux et al., 2012), with most emission occurring in the playa lakes and alluvium deposits near playa lakes (Reheis and Kihl, 1995; Reheis et al., 2009; Urban et al., 2018). Reynolds et al. (2009) observed 71 d with dust plumes during 37 months of camera recording at the Franklin Lake playa. According to remote sensing data (MODIS), aerosol optical depth (AOD) is higher in spring and summer and reaches a minimum in winter (Frank et al., 2007). However, from November to May, eastward flows of the jet stream affect the Mojave Desert, which, in combination with topography, favour the development of northerly winds that can lead to dust emission (Urban et al., 2009). Up to 65 % of emission in the Mojave Desert is estimated to be due to natural factors, whereas 35 % is due to anthropogenic activities, including off-road recreation practices, mine operations, and military training and livestock grazing (Frank et al., 2007). The AOD in this region is also affected by dust transported from other regions (Tong et al., 2012) and pollution transported from the Los Angeles Basin (Frank et al., 2007; Urban et al., 2009). In the Mojave Desert, Reynolds et al. (2009) noted an association between wet periods and dust emission,

directly related to the generation of new, thin crusts and salt crust removal.

The Mojave Desert includes several significant playa lakes, such as Rogers, Rosemond, Owens Lake, Death Valley (Badwater), Panamint Valley, Bristol, Cadiz, Danby, Searles Lake, Soda Lake, and Mesquite Lake (Reheis and Kihl, 1995; Reheis, 1997; Potter and Coppernoll-Houston, 2019). Reynolds et al. (2007, 2009) distinguished between two types of playa lakes, wet playas, influenced by groundwater, and dry playas, unaffected by groundwater, though both can experience surface-water runoff. Goudie (2018) further delineated wet playas as having a groundwater table within 5 m of the surface, while dry playas have a groundwater table deeper than 5 m. Additionally, Goudie (2018), Buck et al. (2011), Nield et al. (2015), and Nield et al. (2016b) observed that the interaction between salt minerals and the groundwater table on wet playas leads to the formation of fluffy surfaces through salt reworking by water during evapotranspiration.

In the Mojave Desert, three different Aridisols are present in the Rand Mountains' alluvial fan, corresponding to xeric soils or Aridisols according to Eghbal and Southard (1993), which are typical in arid and semi-arid regions, with low organic matter content and low structures. The uppermost layer of those Aridisols, ranging from 0 to 1 cm in depth, exhibited a texture of 15 %–30 % gravel, 69 %–74 % sand, and 10 %–11 % clay. Reheis et al. (1995) described soils (< 2 mm) primarily composed of silt (30 %–70 %) and clay (20 %–45 %). The mineralogy of those samples was dominated by quartz, feldspars, amphiboles, and clay minerals, including smectite, mica, and kaolinite (Eghbal and Southard, 1993). The Cronese lakes and Soda Lake playas are documented to contain salt precipitates, but mineralogy is not specified. Mesquite Lake playa is noted for its gypsum deposits (Reynolds et al., 2009). At Franklin Lake playa, surfaces are characterized by silt- and clay-sized particles (Goldstein et al., 2017), with mineralogical descriptions provided in Reynolds et al. (2009) indicating fluffy surfaces comprised of halite, thenardite, trona, burkeite, calcite, illite, smectite, and kaolinite. Similar mineralogical results are described at Soda Lake by Reheis et al. (2009), with a higher proportion of Na salts, quartz, gypsum, and carbonates. Furthermore, Goldstein et al. (2017) identified a diverse array of minerals at Franklin Lake playa, including clays; zeolites; plagioclase; K-feldspar; quartz; calcite; dolomite; and salt minerals such as trona, halite, burkeite, and thenardite.

This study characterizes the particle size distribution, mineralogy, and modes of occurrence of Fe of selected potential dust-emitting sediment surfaces from the Mojave Desert. In addition, the mineralogy of different size fractions is analysed, based on a sieving protocol that minimally disturbs sediments. We further discuss the potential effect of sedimentary transport on the particle size and mineralogy across the sampled basins, building upon previous studies in the literature. Finally, our results are broadly compared with current EMIT standard (semi-quantitative) products and with those

obtained using similar protocols in previous FRAGMENT campaigns in other regions (González-Romero et al., 2023, 2024).

2 Methodology

2.1 Study area

The Mojave Desert, located between California and Nevada, has a diverse geological history spanning from the Cambrian and Precambrian eras to the Holocene (Fig. 1). This geological complexity encompasses volcanic, plutonic, metamorphic, and sedimentary units (Jennings et al., 1962; Miller et al., 2014). In areas once submerged during the Last Glacial Maximum (LGM), we now find ephemeral playa lakes that have existed for thousands of years since the LGM, offering a glimpse into the region's dynamic past (Miller et al., 2018). These playa lakes, together with alluvial fans, floodplains, and other features, are surrounded by a variety of source rocks, exhibit diverse particle sizes and compositions, and can potentially emit dust under favourable wind conditions.

The regional distribution of the annual frequency of occurrence (FoO) of dust events with dust optical depth exceeding 0.1, derived from MODIS Deep Blue C6.1 Level 2 data following the methodology of Ginoux et al. (2012), is illustrated in Fig. 2. The FoO provides an overall estimate of dust emission frequency above a certain threshold at a resolution of $0.1^\circ \times 0.1^\circ$ over the region. Sediment samples were collected from various locations within the Mojave Desert region, including areas with relatively high FoO (see locations in Figs. 1 and 2). Among these locations is Soda Lake and its surroundings, near Baker, CA, which is linked to Silver Lake to the north and is surrounded by igneous, volcanic, and carbonate rocks, as well as dune fields, to the south (Fig. 1). The area is influenced by aeolian, alluvial, and fluvial processes and experiences annual precipitation of 80–100 mm (Urban et al., 2018). This ephemeral lake contains salts resulting from the evaporation of groundwater sourced from an aquifer nestled in the Zzyzx Mountains (Honke et al., 2019). Dust emissions are a recurrent phenomenon, originating from fine sediments accumulated in the lake's central areas during sporadic flooding, from the white evaporite surfaces in the lake, and from the alluvial deposits to the south of the playa lake (Urban et al., 2018). According to the FoO, the areas with higher dust emissions are the southern part of the lake and the alluvial deposits to the southwest, extending up to Afton Canyon.

Samples were also collected from the Cronese lakes, Mesquite Lake, Ivanpah Lake, and Coyote Lake (Fig. 1), which lie in areas with significant FoO signals (Fig. 2) and have been documented as dust sources in Reheis and Kihl (1995) and Reheis et al. (2009). The Cronese lakes are adjacent to the Soda Lake area to the west, sharing a similar geologic context (Figs. 1 and 2). Mesquite Lake, located on the border between California and Nevada, is encircled by car-

bonate and igneous rocks, mirroring the geological setting of the nearby Ivanpah Lake. Notably, Mesquite Lake playa is the only playa affected by a gypsum mine pit, as documented by Reynolds et al. (2009). Further contributing to the diversity of the region's geological makeup is Coyote Lake, flanked by Miocene and Pleistocene sediments. These playa lakes, characterized as endorheic ephemeral lakes, receive groundwater inputs in some cases, enriching the lakes with salts that subsequently precipitate on the surfaces of their central regions (Whitney et al., 2015; Urban et al., 2018).

Other areas with relatively high FoO not sampled in our study include the Ashford Junction alluvial deposits and the Fort Irwin area, where the northern valley, including Nelson Lake, may be more prone to dust emission due to significant anthropogenic disturbance. It is important to note that the FoO may tend to highlight areas such as playas and their surroundings, where in some cases the most dust per unit area could be produced (Floyd and Gill, 2011; Baddock et al., 2016). However, some alluvial regions with lower emission rates not surpassing the FoO threshold may produce more dust overall due to their greater areal extent (Reheis and Kihl, 1995; Baddock et al., 2016). Additionally, many other types of dust-producing surfaces active in the Mojave Desert, such as gravel roads, agricultural lands, and recreational off-road tracks, are rarely observed by satellite retrievals (Urban et al., 2018).

The new EMIT sensor on board the International Space Station offers a glimpse of the mineralogical diversity in the Mojave Desert (Green et al., 2020). Figure 3 displays standard Tetracorder RGB colour composite semi-quantitative products for EMIT. Tetracorder is a software system that employs a set of algorithms within an expert system decision-making framework to identify and map compounds (Clark, 2024; Clark et al., 2024). Figure 3 shows a true colour image, along with standard products for mineral electronic absorption bearing Fe^{2+} and Fe^{3+} (including hematite and goethite) in the visible to very near infrared spectral range. It also displays standard products for the EMIT-targeted minerals, excluding hematite and goethite: calcite, chlorite/serpentine, dolomite, gypsum, illite/muscovite, kaolinite-dioctahedral group, montmorillonite group, and vermiculite. These products highlight areas where the presence of each mineral or component is significant, measured in terms of band depth fit, where the fit represents the least squares correlation coefficient from a feature fit of observed and reference library spectra. These analyses reveal the widespread presence of phyllosilicates such as kaolinite, smectite, montmorillonite, and illite across the area. The northeastern sector, particularly around Mesquite Lake, exhibits notable concentrations of carbonates and gypsum. Additionally, goethite and hematite are detected, with a more pronounced presence of goethite in the northern portion and hematite in the southern part of the region. The detection of mixtures of Fe^{2+} and Fe^{3+} within various minerals enriches our understanding of the region's mineralogical diversity.

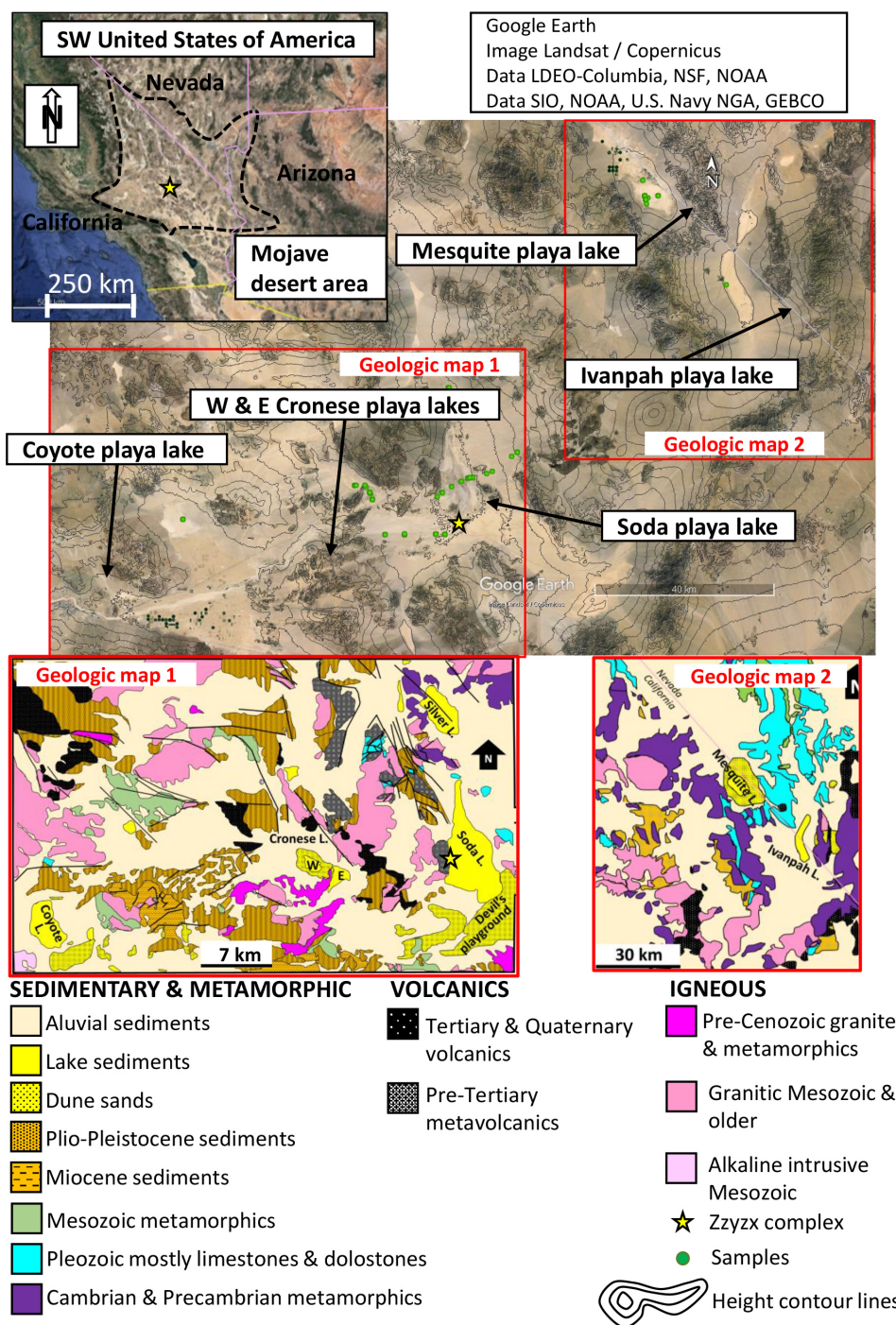


Figure 1. Study area map including the playa lakes studied together with a geologic map, simplified from Jennings et al. (1962) and Miller et al. (2014). The star represents the Zzyzx complex and green dots the samples used in this study. Basemap: imagery data from © Google Earth Pro v: 7.3.6.9345.

Quantitative surface mineralogy (mineral mass abundances of the 10 EMIT-targeted minerals) and soil texture products are currently being developed by the EMIT team for use in Earth system models. Their publication and evaluation will be the focus of forthcoming publications. Thus, it is

beyond the scope of this study to perform a detailed quantitative comparison between our analyses and comparable EMIT products. However, in the Results section, we broadly compare these standard products with the results of our in situ analyses.

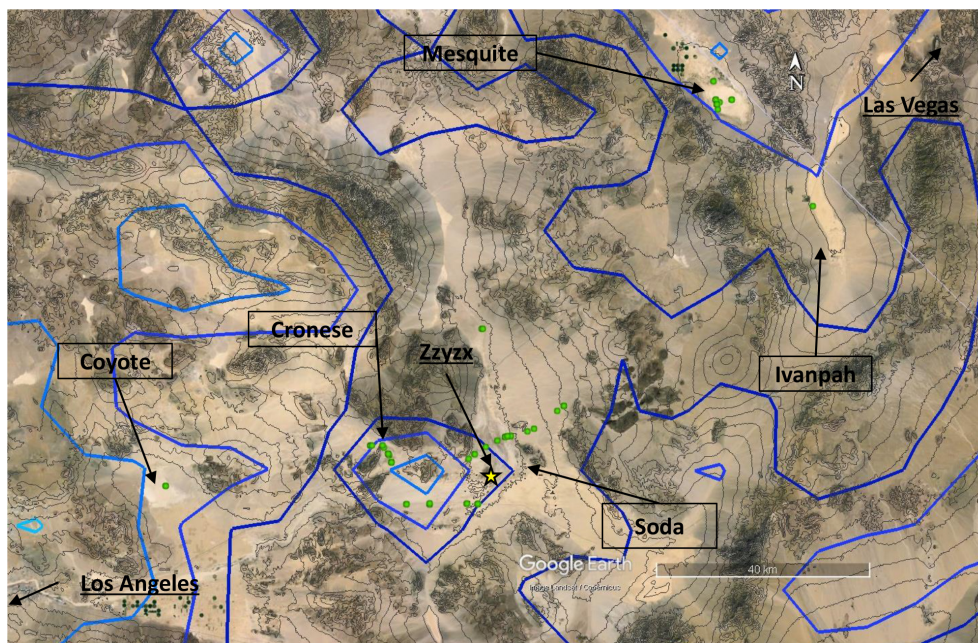


Figure 2. Map of frequency of occurrence (FoO) of dust optical depth (DOD) > 0.1 over the study region derived from MODIS C6.1 Aqua (13:30 LT equatorial passing time) Level 2 Deep Blue aerosol products at 0.1° resolution. A dust occurrence is counted when $\text{DOD} > 0.1$, Ångström exponent < 0.3 , and $\text{DOD at } 412 \text{ nm} > \text{DOD at } 470 \text{ nm}$. Blue iso-contours represent 5 % and 10 % of daily occurrences per year averaged over 20 years (2003–2022). Green dots represent the samples collected and used in this study. Basemap: imagery data from © Google Earth Pro v: 7.3.6.9345.

2.2 Sampling

Representative surfaces of dust-emitting sediments were sampled in May 2022, with depths of up to 3 cm, using a 5 cm^2 inox shovel. Samples were stored in a plastic bag; labelled; documented with photographs, descriptions, and coordinates; and transported to the laboratories for subsequent analyses. The type of samples considered is crusts (semi-cohesive fine sediments accumulated during flooding in depressions) and ripples (aeolian ripples that are built up under favourable winds and supply sand for saltation) (Fig. 4). A total of 55 surface sediments and ripples (32 from Soda Lake, 9 from Mesquite Lake, 1 from Ivanpah Lake, 11 from the Cronese lakes, and 2 from Coyote Lake) were sampled for laboratory analysis. Once in the laboratory, the samples were dried for 24–48 h at $40\text{--}50^\circ\text{C}$ and sieved to pass through a 2 mm mesh.

Our rationale for selecting crusts and ripples is twofold. On the one side, dust emission is primarily driven by two mechanisms: saltation bombardment and aggregate disintegration. In saltation bombardment, dust is ejected from soil aggregates (typically crusts and paved sediments rich in clay and silt particles) when impacted by saltating sand particles. In aggregate disintegration, dust is released from saltating soil aggregates (Shao et al., 1993; Alfaro et al., 1997; Shao, 2001). By characterizing the PSD (both dry- and wet-sieved) and mineralogy of ripples (concentrating sand par-

ticles) and crusts (concentrating clay and silt particles), we provide comprehensive and valuable information for developing and refining dust emission models. On the other side, in arid regions, quartz and feldspar typically dominate sediment mass. However, current spaceborne hyperspectral instruments (such as EMIT) cannot directly identify feldspar and quartz because their absorption features lie outside the instrument's spectral range. This poses a significant challenge in quantifying surface mineral abundances from remote spectroscopy. At all FRAGMENT sampling locations (Morocco, Iceland, Mojave in the USA, and Jordan), we measured reflectance spectra using an ASD FieldSpec3. By characterizing and contrasting ripples (with high quartz and feldspar content and larger particle sizes) and crusts, we aim to provide information to enhance understanding and improve modelling assumptions for estimating surface mineral abundances and soil texture from remote spectroscopy in subsequent studies.

We acknowledge that the limited number of samples collected may not fully represent the potential variability among crusts and ripples within the studied locations due to varying conditions (Buck et al., 2011). However, our samples broadly represent the composition and particle size distributions (PSDs) of this type of sediment in these areas, allowing for meaningful comparisons with sediments from other locations.

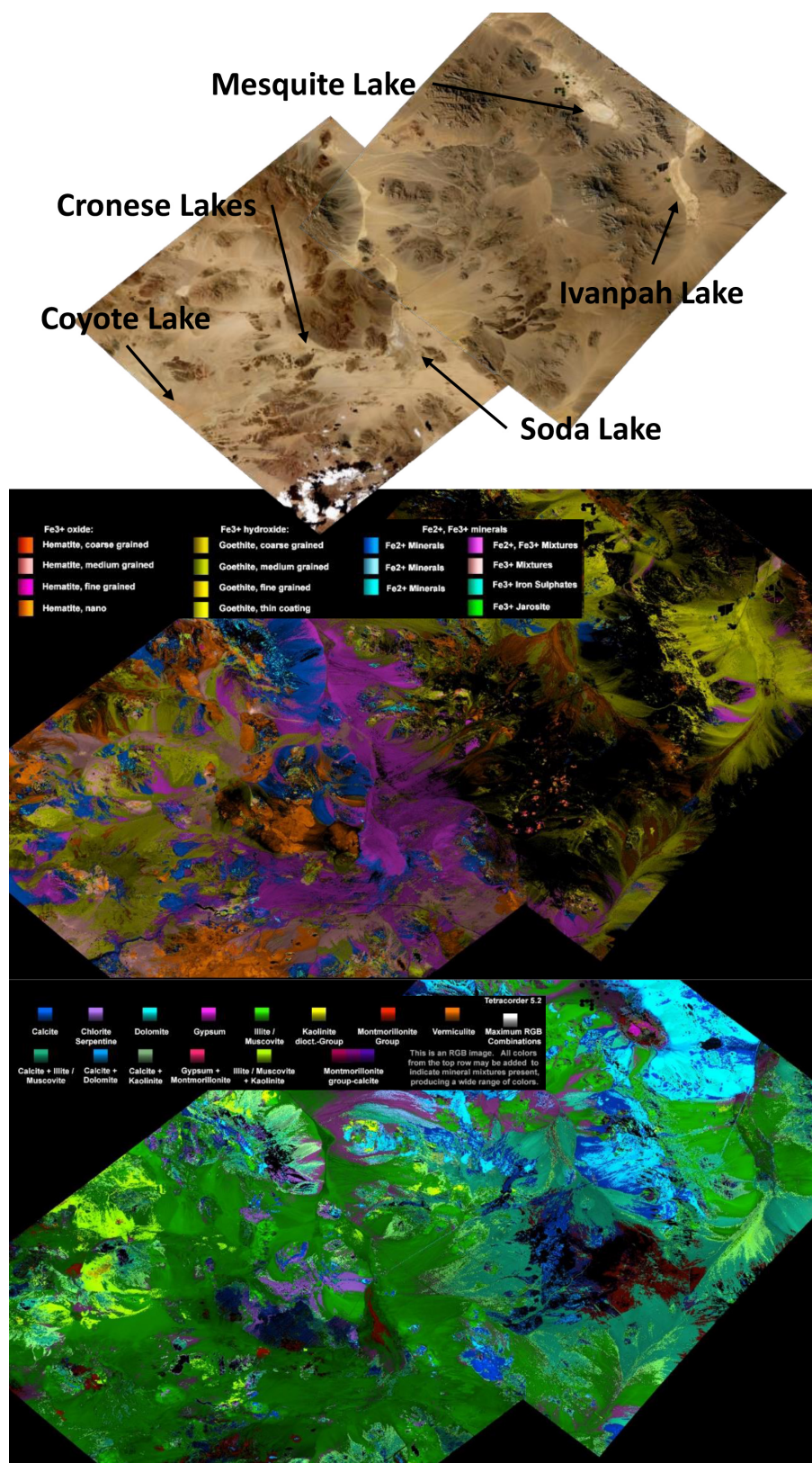


Figure 3. EMIT scenes emit20231015T215209_color-visRGB and emit20230728T214142_color-visRGB at 60 m px^{-1} showing the diversity of Fe^{2+} , Fe^{3+} , and minerals bearing Fe^{2+} and Fe^{3+} and the carbonate, salt, and phyllosilicate minerals.

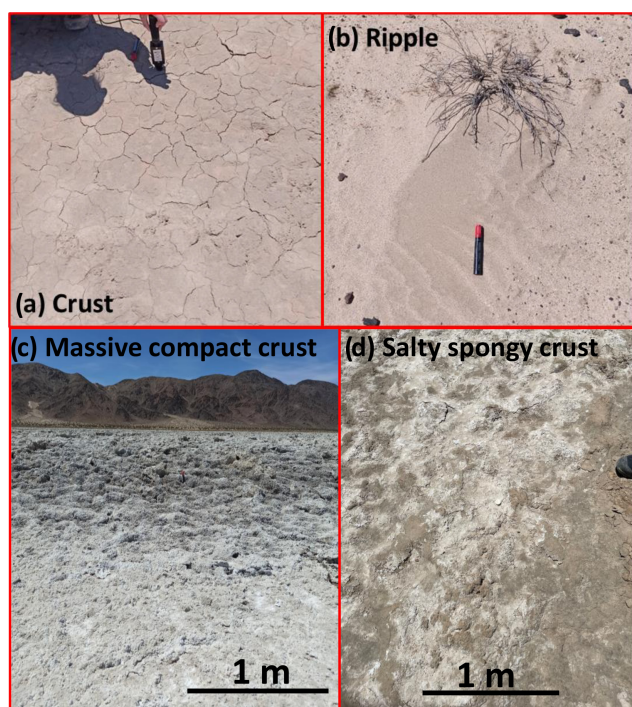


Figure 4. Examples of samples collected in the Mojave Desert including crusts (a); aeolian ripples (b); a massive compact crust (c); and a salty, spongy crust (d).

2.3 Analyses

2.3.1 Particle size distribution

Particle size distributions (PSDs) of bulk samples (< 2 mm) were analysed as described in González-Romero et al. (2023) for the evaluation of the aggregation state. First, we conducted a minimally dispersed PSD (MDPSD) analysis, which minimizes the breaking of the aggregates that are encountered in natural conditions. Second, we conducted a fully dispersed PSD (FDPSD) analysis, which breaks the aggregates. Wet dispersion was done according to Sperazza et al. (2004), using water and sodium hexametaphosphate dispersion for 24 h. Both PSDs (MDPSD and FDPSD) were obtained by a laser diffractometer with the Malvern Mastersizer 2000 Hydro G and Scirocco for the fully and minimally dispersed conditions, respectively. We note that under wet dispersion, at least some salt minerals may dissolve.

In addition, we separated 20 selected samples from different sources, including 16 crusts and 4 aeolian ripples, into different size ranges to understand how mineral composition changes with size. We used a series of sieves with mesh sizes of 2 mm, 1 mm, 500 μm , 250 μm , 80 μm , 63 μm , 40 μm , and 20 μm . The sieving process involved hand-shaking the full column for 1 min, followed by ultrasound sonication for 1 min for the 500, 80, 40, and 20 μm size fractions. This method ensured the effective separation of the size fractions for subsequent mineralogical analysis.

2.3.2 Mineralogical composition

To quantify the different contents of crystalline minerals and amorphous components, X-Ray diffraction (XRD), coupled with a Rietveld quantitative method, was used (Rietveld, 1969; Cheary and Coelho, 1992; Young, 1993; TOPAS, 2018). Adding a known amount of an internal standard material allowed, via the Rietveld method, the quantification of a mixture of minerals and any non-crystalline material in the mixture not included in the Rietveld method (De la Torre et al., 2001; Madsen et al., 2001; Scarlett and Madsen, 2006; Machiels et al., 2010; Ibañez et al., 2013). For the analysis, a measured amount of dry-ground sample was mixed and dry-ground again with 10 %–20 % of fluorite (CaF_2 powder, Merck), used here as an internal standard for quantitative purposes. The XRD patterns of the samples were analysed by a Bruker D8 A25 ADVANCE powder X-ray diffractometer operated at 40 kV and 40 mA with monochromatic $\text{Cu K}\alpha$ radiation ($= 1.5405 \text{ \AA}$). This device uses a Bragg–Brentano geometry and a LynxEye 1D sensitive detector. Diffractograms were recorded from 4 to 120° of 2θ and steps of 0.015° in 1 s and maintained rotation (15 min^{-1}). For the clay identification, samples were analysed using the oriented aggregate method by XRD, decanting clay fractions from samples and smearing the slurries in glass slides. After, three treatments were applied including air drying (AO), glycolation with ethylene glycol (AG), and heating at 550°C for 2 h (AC) with its three different diffractograms. Finally, the three diffractograms allow us to corroborate the presence of illite, chlorite, palygorskite, and montmorillonite through Thorez (1976) and USGS (2024) procedures. Data collected were evaluated using the Bruker AXS DIFFRAC.EVA software package (Bruker AXS, Karlsruhe, Germany, 2000), and the Rietveld analyses were performed with the TOPAS 4.2 program (Bruker AXS, 2003–2009). A Chebyshev function of level 5 was used to fit the background, and abundances of crystalline and amorphous phases were normalized to 100 %. Fits were evaluated by visual comparison, i.e. R_{wp} (R -weighted pattern), R_{exp} (R -expected), and goodness of fit (GOF).

2.3.3 Mode of occurrence of Fe

As XRD is not precise enough for Fe-oxide quantification, wet chemistry and sequential extractions of Fe are needed for quantification of the mode of occurrence of Fe (González-Romero et al., 2023, 2024). Samples were analysed with a two-step acid digestion for the total Fe (FeT) content following Querol (1993, 1997). A reference material (NIST-1633b, coal fly ash) was used for quality control in every batch. The sequential extraction presented in Shi et al. (2009), Baldo et al. (2020), and González-Romero et al. (2024) was used to quantify readily exchangeable Fe ions and nano-sized Fe oxides (FeA), the amount of crystalline Fe oxides as goethite and hematite (FeD), and crystalline magnetite (FeM). For

the first extraction, 30 mg samples were leached with 10 mL of an ascorbate solution (extractant solution) and shaken in dark conditions for 24 h and filtered. Another 30 mg was leached with 10 mL of a dithionite solution (extractant solution), shaken for 2 h in dark conditions, and filtered for the second extraction. The solid residue was then leached again in 10 mL of an oxalate solution for 6 h in dark conditions and filtered for the third extraction. The extracted solution of each phase (FeT, FeA, FeD, and FeM) was analysed to quantify dissolved Fe by inductively coupled plasma atomic emission spectrometry (ICP-AES). FeA is obtained with the first extraction, and FeD is obtained by subtracting the amount of Fe from the first extraction from the second extraction. Finally, the FeM is related to the third extraction. At the end, the equivalent to the Fe as structural Fe was obtained, $FeS = FeT - FeA - FeD - FeM$, which is included in other minerals and amorphous phases. To test accuracy, 30 mg of Arizona Test Dust (ATD; ISO 12103-1, A1 Ultrafine Test Dust; Powder Technology Inc.) was subjected to the same extraction procedure in every batch and extraction.

The average Fe content of the reference material 1633b was $7.6 \pm 0.5\%$ (certified 7.8%). Furthermore, the average values of the sequential Fe extraction of the ATD reference material were $0.073 \pm 0.012\%$, $0.47 \pm 0.01\%$, and $0.042 \pm 0.002\%$ for FeA, FeA+FeD, and FeM, respectively, while the certified contents are 0.067% , 0.48% , and 0.047% , respectively.

3 Results

3.1 Particle size distribution

The PSD and median particle diameter of fully and minimally disturbed samples are key parameters for understanding the cohesion and aggregation state of sediments (González-Romero et al., 2024). We note that in the Mojave Desert, some basins are enriched in salts, which can cause some artefacts in the FDPSD. The dissolution of salts during wet dispersion for bulk PSD analysis (< 2 mm) can remove aggregating agents. This salt cementation of the crusts might reduce the dust emission potential of the surface.

The average PSDs of crusts across different basins exhibit remarkable similarity, yet disparities between FDPSDs and MDPSDs are pronounced, indicating varying degrees of particle cohesion and aggregation at Cronese, Mesquite, Ivanpah, and Coyote lakes. In these locations, FDPSDs feature a dominant mode at $8\text{--}10\ \mu\text{m}$ alongside a coarser mode at $100\ \mu\text{m}$, while MDPSDs are characterized by a dominant coarser mode (Fig. 5). In contrast, Soda Lake crusts exhibit similarity between FDPSDs and MDPSDs. Average FDPSDs and MDPSDs of aeolian ripples from the Mojave Desert are found to be similar, typically featuring a major size mode between 100 and $300\ \mu\text{m}$. However, distinctions arise when analysing specific lakes. Aeolian ripples from Soda, Cronese, and Coyote lakes showcase a dominant coarse mode at 200--

$300\ \mu\text{m}$, whereas those from Mesquite Lake show a dominant mode at a finer scale, approximately at $100\ \mu\text{m}$ (Fig. 5).

The crusts' means of all median particle diameters (mean median) in the analysed Mojave Desert dust source sediments reveal a coarser MDPSD compared to the FDPSD, with values of 92 and $37\ \mu\text{m}$, respectively. In contrast, the mean median particle diameter is similar for aeolian ripples (226 and $213\ \mu\text{m}$, respectively) (Table S1 in the Supplement). Analysing specific locations, the mean median particle diameter from the MDPSD of crusts varies, with the finest crust observed at Ivanpah Lake ($35\ \mu\text{m}$) and the coarsest at Mesquite Lake ($141\ \mu\text{m}$). For the FDPSD, the finest crust originates from Coyote Lake ($8.4\ \mu\text{m}$), while the coarsest is from Soda Lake ($52\ \mu\text{m}$) (Table S1). Similarly, for aeolian ripples, the mean median particle diameters for both the MDPSD and FDPSD are finer at Mesquite Lake (167 and $67\ \mu\text{m}$, respectively) and coarser at Cronese lakes (264 and $234\ \mu\text{m}$, respectively) (Table S1). The high degree of particle aggregation observed in crusts, contrasting with the lower aggregation state in ripples, aligns with findings reported for dust-emitting sediments from Morocco by González-Romero et al. (2023).

The mean median particle diameters of crusts collected in the Mojave Desert are similar to those from Morocco described by González-Romero et al. (2023). Specifically, the mean median MDPSD diameter for the Mojave Desert ($92 \pm 74\ \mu\text{m}$) closely resembles that of the Lower Draâ basin in Morocco ($113 \pm 79\ \mu\text{m}$), albeit slightly finer, and is notably coarser than that of Iceland ($55 \pm 62\ \mu\text{m}$) (González-Romero et al., 2023, 2024). Furthermore, the finest crust sampled in the Mojave Desert (Ivanpah with $35\ \mu\text{m}$) is almost twice as coarse as the finest from Morocco (L'Bour with $20\ \mu\text{m}$). For the FDPSD, the Icelandic top sediment surface is the coarsest ($56 \pm 69\ \mu\text{m}$), followed by both Morocco and Mojave crusts (37 ± 77 and $37 \pm 48\ \mu\text{m}$, respectively). Additionally, average MDPSD median diameters of aeolian ripples from the Mojave Desert source samples closely resemble those from Morocco (226 and $221\ \mu\text{m}$, respectively), while those from Iceland are slightly coarser ($280\ \mu\text{m}$).

Dry-sieved size fractions of dust-emitting sediments show the highest percentage of mass in the $250\text{--}500$ and $80\text{--}250\ \mu\text{m}$ fractions, with minimal mass within $500\text{--}1000\ \mu\text{m}$, $1\text{--}2$ mm, and the finer fractions ($20\text{--}40$ and $< 20\ \mu\text{m}$) (Fig. 6, Table S2). In both cases, the size fractions from 80 to $500\ \mu\text{m}$ accumulated a total of 75% to 90% of the total mass fraction (Table S2).

Close to the centre of the Soda Lake, where numerous crust samples were collected, before reaching massive crust cementation by evaporite minerals, the FDPSD median diameter reaches very fine sizes ($8\text{--}15\ \mu\text{m}$) (Fig. S1 in the Supplement). In contrast, towards the edges of the basin (closer to the mountains surrounding this endorheic lake), the size markedly increases, ranging from 22 to $87\ \mu\text{m}$ (Fig. S1). Similar patterns, yet with coarser sizes, are observed for the MDPSD. As described in previous studies, the fluctuation of

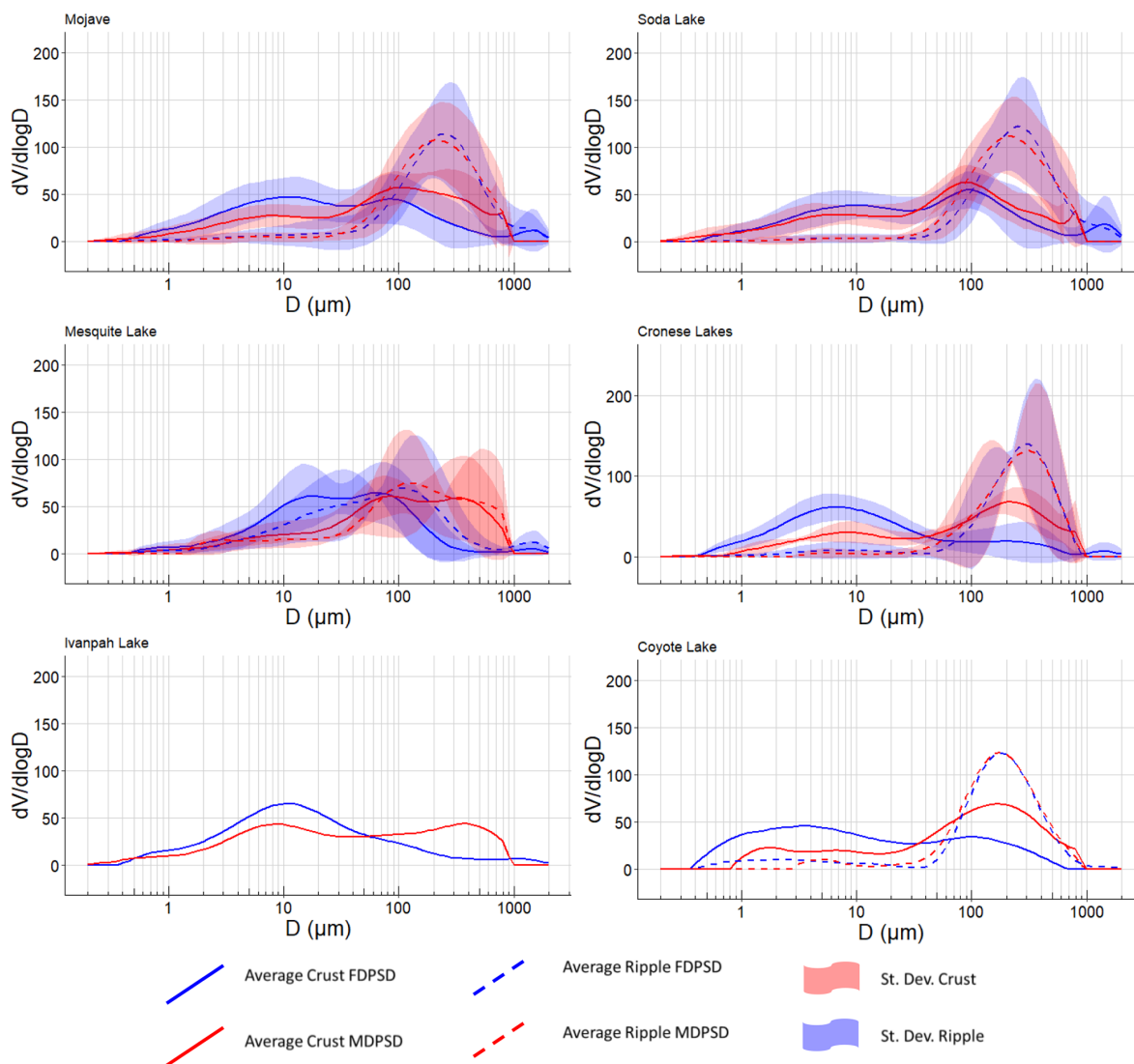


Figure 5. Fully dispersed particle size distribution (FDPD) and minimally dispersed particle size distribution (MDPSD) for crusts and aeolian ripples from the Mojave Desert (median PSD from all the samples) and Soda, Mesquite, Cronese, Ivanpah, and Coyote lakes. In purple and pink shading, the standard deviation of each PSD is shown (no. of samples used in Table 1), except for Ivanpah and Coyote lakes (only one sample each).

the groundwater table in the centre of the basin can lead to a massive precipitation of salts, resulting in the formation of compact crusts (Fig. 4) (Reynolds et al., 2007; Nield et al., 2016a, b; Urban et al., 2018) that should effectively reduce dust emission. However, at the edges, where the precipitation of salts is less frequent and reworking of the crusts by fluctuations in the groundwater table occurs, salty and spongy crusts are formed (Fig. 4) (Nield et al., 2016a, b). These spongy crusts, being less compact, are more easily broken by saltating particles, potentially leading to high-salt dust emissions.

The slight particle size segregation, with finer particles accumulating towards the centre of the lake, can be attributed to the transport of sediments from the surrounding mountains

to the lake's centre by runoff waters during rain episodes. Initially, the coarser particles are deposited, followed by the finer particles that remain suspended in the water for a longer duration. Nevertheless, the crusts in the surroundings alluvial fans of the Soda Lake are fine enough (22–87 μm in the edges compared to 8–15 μm in the centre; Fig. S1) and surrounded by dunes (availability of saltators for saltation bombardment) to have a high potential dust emission under favourable conditions (Reynolds et al., 2006; Reheis et al., 2009; Urban et al., 2018).

Table 1. Full range (< 2000 μm), < 63 μm , and > 63 to 2000 μm mean diameter and standard deviation (SD), min, and max for minimally dispersed particle size distribution (MDPSD) and fully dispersed particle size distribution (FDPSD). NaN: not a number.

Surface	Location	N	MDPSD		
			Full range	$\leq 63 \mu\text{m}$	> 63 to 2000 μm
			Mean of medians \pm SD [min, max]		
Crusts	Mojave	35	92 \pm 74 [10, 349]	22 \pm 6.4 [11, 34]	254 \pm 71 [155, 489]
Ripples		20	226 \pm 88 [88, 418]	37 \pm 6.0 [20, 46]	276 \pm 80 [130, 424]
Crusts	Soda	17	63 \pm 47 [10, 156]	21 \pm 6.5 [11, 31]	234 \pm 82 [155, 489]
	Cronese	9	109 \pm 60 [35, 195]	18 \pm 2.2 [15, 22]	280 \pm 40 [238, 357]
	Mesquite	7	141 \pm 117 [31, 349]	28 \pm 5.6 [21, 34]	257 \pm 79 [157, 387]
	Ivanpah	1	35 \pm NaN [35, 35]	16 \pm NaN [16, 16]	314 \pm NaN [314, 314]
	Coyote	1	101 \pm NaN [101, 101]	20 \pm NaN [20, 20]	254 \pm NaN [254, 254]
Ripples	Soda	15	231 \pm 87 [88, 418]	39 \pm 3.5 [29, 43]	275 \pm 77 [130, 424]
	Cronese	2	264 \pm 147 [160, 368]	40 \pm 8.8 [34, 46]	292 \pm 120 [208, 377]
	Mesquite	2	167 \pm 112 [110, 225]	26 \pm 8.9 [20, 32]	286 \pm 146 [183, 389]
	Ivanpah	0	NaN	NaN	NaN
	Coyote	1	179 \pm NaN [179, 179]	32 \pm NaN [32, 32]	236 \pm NaN [236, 236]
Surface	Location	N	FDPSD		
			Full range	$\leq 63 \mu\text{m}$	> 63 to 2000 μm
			Mean of medians \pm SD [min, max]		
Crusts	Mojave	35	37 \pm 48 [4.9, 240]	18 \pm 6.6 [8.4, 35]	306 \pm 237 [106, 1093]
Ripples		20	213 \pm 92 [28, 362]	29 \pm 8.3 [15, 48]	335 \pm 99 [213, 561]
Crusts	Soda	17	52 \pm 61 [8.4, 240]	19 \pm 5.3 [12, 27]	321 \pm 212 [113, 815]
	Cronese	9	17 \pm 23 [4.9, 77]	12 \pm 3.1 [8.4, 19]	381 \pm 345 [144, 1093]
	Mesquite	7	34 \pm 28 [11, 91]	24 \pm 7.7 [16, 35]	185 \pm 104 [106, 336]
	Ivanpah	1	12 \pm NaN [21, 21]	15 \pm NaN [15, 15]	347 \pm NaN [347, 347]
	Coyote	1	8.4 \pm NaN [8.4, 8.4]	12 \pm NaN [12, 12]	187 \pm NaN [187, 187]
Ripples	Soda	15	234 \pm 82 [92, 362]	31 \pm 7.9 [21, 48]	346 \pm 97 [238, 561]
	Cronese	2	236 \pm 126 [147, 325]	18 \pm NaN [18, 18]	295 \pm 108 [219, 371]
	Mesquite	2	67 \pm 56 [28, 107]	27 \pm 3.5 [24, 29]	336 \pm 173 [213, 458]
	Ivanpah	0	NaN	NaN	NaN
	Coyote	1	156 \pm NaN [156, 156]	15 \pm NaN [15, 15]	245 \pm NaN [245, 245]

3.2 Mineralogy

Dust-emitting sediments from the Mojave Desert primarily consist of feldspars (41 \pm 12 %, including albite/anorthite and microcline), quartz (22 \pm 11 %), and clay minerals (18 \pm 12 %, such as kaolinite, montmorillonite, and illite). Additionally, minor contents of carbonate minerals (6.6 \pm 6.6 %), amphiboles (pargasite) (4.1 \pm 1.5 %), and iron oxides (maghemite/magnetite) (0.77 \pm 0.54 %) are observed (Fig. 7, Tables 2 and S3). At Soda, Mesquite, and Cronese lakes, Na salts such as halite, thenardite, trona, and burkeite are also present, with an average salt content of 5.0 \pm 11 %. Additionally, zeolites (0.77 \pm 1.1 % to 8.5 %) including laumontite and analcime are detected at Soda, Cronese, and Coyote lakes (the southern sites), with the highest content observed at Coyote Lake. High amounts of gypsum are found at Mesquite Lake (15 \pm 29 %) (Fig. 7, Tables 2 and S3).

Moreover, Mesquite Lake crusts exhibit high contents of dolomite and calcite (15 \pm 11 %) compared to other basins (3.6 \pm 2.6 % to 7.2 %) (Table 2).

The overall mineral composition of the dust-emitting sediments originates primarily from the source rocks prevalent in the region. These include dominant Mesozoic granitic rocks, as well as pre-Tertiary, Tertiary, and Quaternary volcanic rocks, and Pre-Cambrian and Mesozoic metamorphic rocks (Fig. 1). In the northern, northeastern, and eastern areas of Mesquite Lake, an important limestone and dolostone massif from the Palaeozoic era contributes notably to the high content of calcite and dolomite in the sediments of this lake (Fig. 1). Zeolite content in the sediments may be attributed to the weathering of volcanic outcrops in the region or to precipitation in alkaline lakes. This diverse bedrock mineralogy results in a wide variety of minerals in the dust-

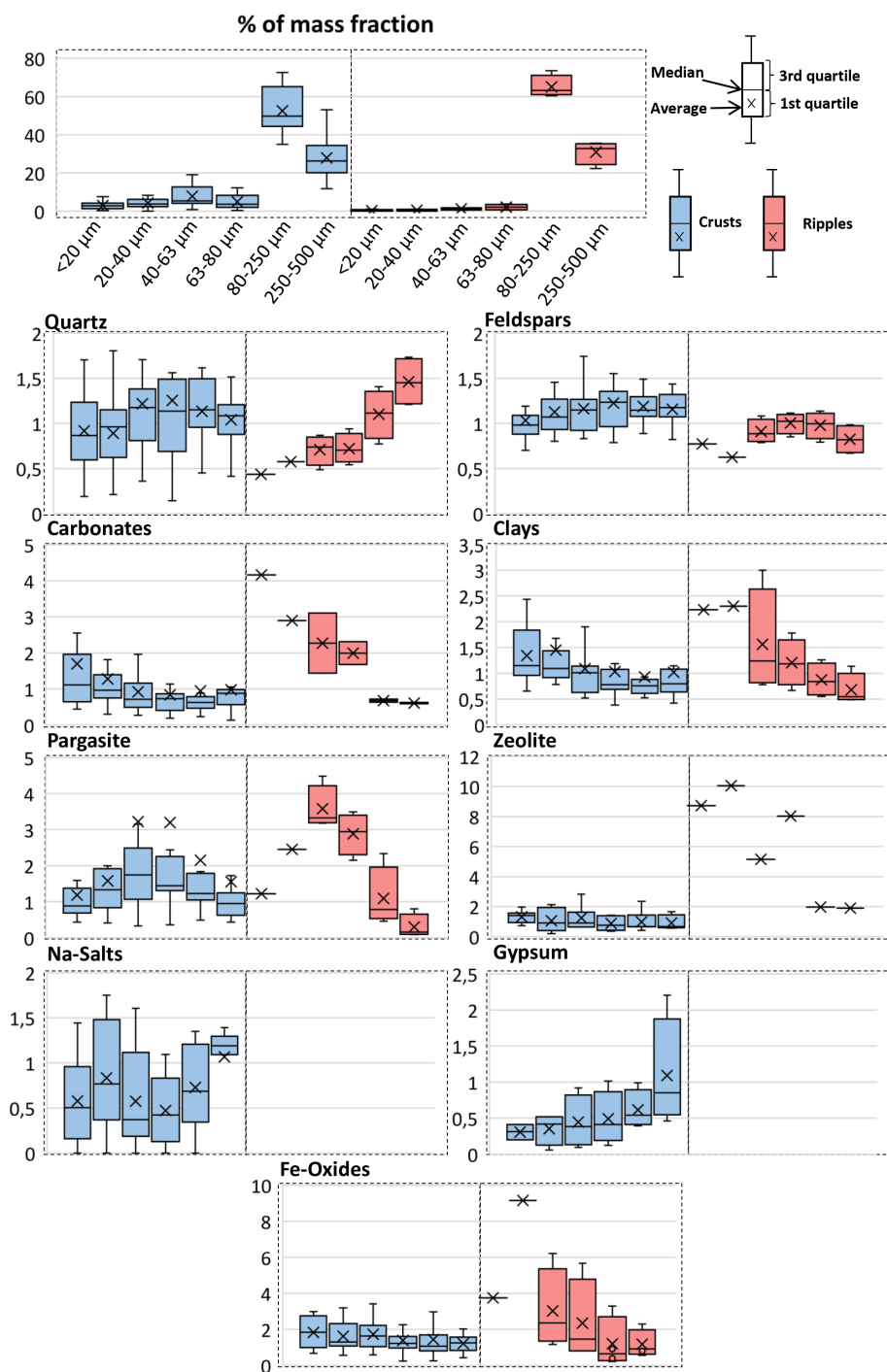


Figure 6. Percentage of mass fractions from the dry-sieved size fractions (250–500, 80–250, 63–80, 40–63, 20–40, and < 20 μm). The range of the enrichment factors of each mineral group for each dry size fraction of the 16 crust samples (blue) and of the 4 aeolian ripple samples (red).

emitting sediments. The form of iron oxide detected in the samples, identified via XRD, is maghemite. However, distinguishing between maghemite and magnetite using XRD is challenging (Vandenberghe et al., 2000), and magnetite has been found to be ubiquitous in Mojave dust (Reheis

et al., 2009; Reynolds et al., 2006). Therefore, we refer to “maghemite/magnetite” to account for the potential presence of both minerals in the samples. In comparison to aeolian ripples, the average composition of the crusts shows enrichment in clay minerals ($24 \pm 11\%$ vs. $7.8 \pm 2.3\%$

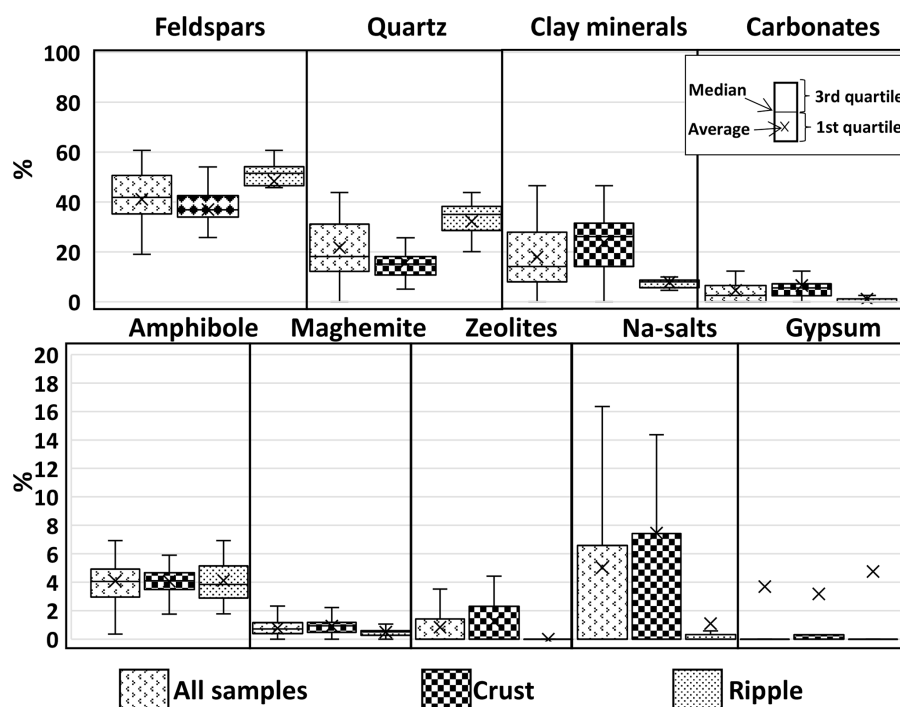


Figure 7. Box plot showing average mineral contents for all samples, crusts, and aeolian ripples (wt %).

Table 2. Average and standard deviations of the mineral contents (wt %) from crust and aeolian ripple samples from the Mojave Desert and the different study basins. Maghemite denotes the potential presence of both maghemite and magnetite. NaN: not a number.

	Clays	Carbonate	Salts	Zeolites	Maghemite	Quartz	Feldspars	Gypsum	Amphiboles
Crusts	24 ± 11	6.6 ± 6.6	7.3 ± 13	1.2 ± 1.9	0.92 ± 0.59	16 ± 7.2	37 ± 9.7	3.1 ± 14	4.1 ± 1.5
Soda	22 ± 11	3.6 ± 2.6	8.9 ± 17	0.77 ± 1.1	0.97 ± 0.66	18 ± 7.7	40 ± 6.7	0.29 ± 0.68	4.5 ± 1.6
Cronese	31 ± 11	5.4 ± 1.8	2.2 ± 3.4	2.4 ± 1.7	1.0 ± 0.28	14 ± 7.3	40 ± 5.5	< 0.1	3.4 ± 1.5
Coyote	28	7.2	1.2	8.5	0.48	11	37	< 0.1	5.6
Ivanpah	36	6.9	< 0.1	< 0.1	1.2	15	36	< 0.1	3.5
Mesquite	17 ± 8.2	15 ± 11	12 ± 14	< 0.1	0.71 ± 0.75	14 ± 5.8	24 ± 12	15 ± 29	2.8 ± 1.4
Ripples	7.8 ± 2.3	1.1 ± 2.2	1.1 ± 3.7	0.12 ± 0.52	0.49 ± 0.28	32 ± 9.5	48 ± 13	4.7 ± 20	4.1 ± 1.6
Soda	7.4 ± 1.8	0.47 ± 0.73	0.19 ± 0.46	< 0.1	0.49 ± 0.25	35 ± 4.5	52 ± 4.7	< 0.1	4.3 ± 1.5
Cronese	8.4 ± 0.60	1.2 ± 1.7	< 0.1	< 0.1	0.83 ± 0.33	32 ± 9.0	53 ± 0.03	< 0.1	4.7 ± 3.2
Coyote	7.9	2.3	< 0.1	2.3	0.60	28	52	< 0.1	3.5
Ivanpah	NaN	NaN	NaN	NaN	NaN	NaN	NaN	NaN	NaN
Mesquite	10 ± 6.1	4.8 ± 6.8	9.4 ± 9.9	< 0.1	0.19 ± 0.27	10 ± 14	15 ± 21	47 ± 60	3.7 ± 1.5

in crust and ripples, respectively), carbonates ($6.6 \pm 6.6\%$ vs. $1.1 \pm 2.2\%$), Na salts ($7.3 \pm 13\%$ vs. $1.1 \pm 3.7\%$), zeolites ($1.2 \pm 1.9\%$ vs. $0.12 \pm 0.52\%$), and maghemite/magnetite ($0.92 \pm 0.59\%$ vs. $0.49 \pm 0.28\%$), while being depleted in quartz ($16 \pm 7.2\%$ vs. $32 \pm 9.5\%$), feldspars ($37 \pm 9.7\%$ vs. $48 \pm 13\%$), and gypsum ($3.1 \pm 14\%$ vs. $4.7 \pm 20\%$) and showing a similar amphibole content ($4.1 \pm 1.5\%$ vs. $4.1 \pm 1.6\%$) (Fig. 7, Tables 2 and S3). These mineral enrichment and depletion trends in crusts are observed in all the playa lakes, except for Mesquite Lake, which is discussed below.

In Soda Lake, the concentration of Na salts in crusts increases towards the inner part of the lake, ranging from 5%–10% at the margins to 45%–50% in the centre, where compact and fully salt-cemented crusts form. This phenomenon is illustrated in Fig. 8, which presents a geological and mineralogical cross-section of Soda Lake. In addition to the water transport to this central part of the basin during the rain episodes, groundwater discharge from the Zzyzx Mountains occurs. There, the groundwater table is close to the surface, and its interaction with the surface causes the massive mobilization of Na salts that consolidate the crusts (Fig. 4) (Nield

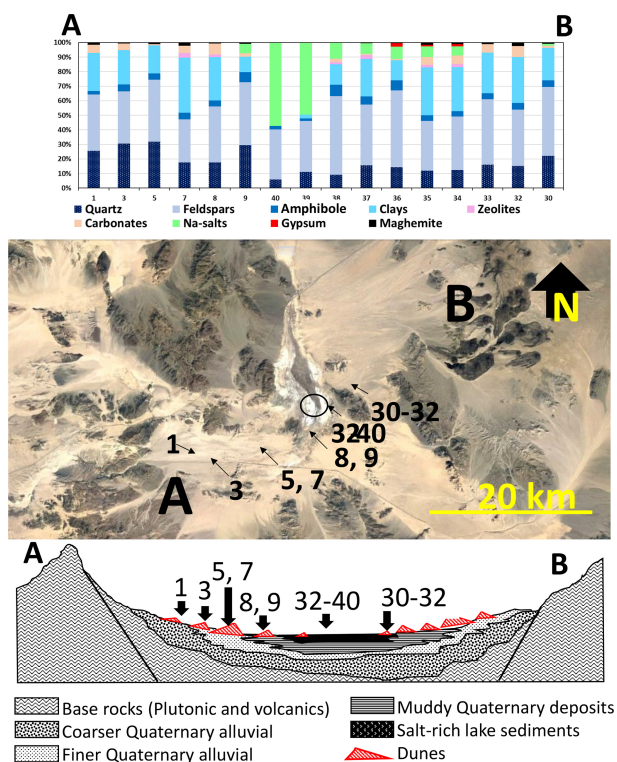


Figure 8. Geological cross-section and mineralogy of the crusts of the Soda Lake. The top panel represents major mineralogy composition. The middle panel represents the position of the samples, the Zzyzx complex, and the path of the cross-section. The bottom panel shows a schematic cross-section simplifying the position in the basin. Basemap: imagery data from © Google Earth Pro v: 7.3.6.9345.

et al., 2016b). Cycles of precipitation and dissolution of the salts yield salty, spongy crusts (Fig. 4) at the edges of these massive crusts, with higher dust emission potential in the degraded salty crusts (Nield et al., 2016a). The very high content of Na salt content in Soda Lake is attributed to the continuous high Na–S–Cl groundwater interaction in the vicinity of Zzyzx, defining Soda Lake as a wet playa lake according to Reynolds et al. (2009) and Urban et al. (2018). On the other hand, Cronese, Coyote, and Ivanpah are categorized as dry lakes.

Mesquite Lake features extensive gypsum deposits at the surface, which are a major component of both dunes and crusts. A small gypsum mine operates in Mesquite Lake. The gypsum content in crusts is notably higher at the centre (80%) compared to the margins (3%–11%). In contrast, the contents of Na salts and carbonates are greater at the margins (30% and 12%–18%, respectively) than at the centre (7.5%–14% and < 0.1%–6.9%, respectively). Aeolian ripples at the centre of Mesquite Lake exhibit a very high gypsum content, whereas at the margins, these ripples contain higher amounts of quartz, feldspars, and clays than at the centre. Despite the presence of the disturbed mine area, most

large dust events at Mesquite Lake have been observed to originate from natural (undisturbed) playa surfaces near the margins (Richard Reynolds, personal communication, 2024).

Amphiboles in the Mojave Desert, sourced from metamorphic rocks in the area, are homogeneous and can serve as a marker for emitted desert dust in the region. Comparing mineralogy of Mojave Desert crusts to Moroccan surface samples (González-Romero et al., 2023), the former are largely enriched in feldspars, clay minerals, Na salts, and gypsum and depleted in quartz and carbonates, with trace proportions of amphiboles, zeolites, and maghemite/magnetite. Ripples in the Mojave Desert are depleted in quartz and carbonates and enriched in feldspars, clay minerals, Na salts, and gypsum, with traces of amphiboles, maghemite/magnetite, and zeolites compared to Moroccan ripples. The mineralogy of the Mojave Desert is markedly different from that of Iceland, due to differences in bedrock geology, although both contain feldspars, zeolites, and maghemite/magnetite (González-Romero et al., 2024).

Particle aggregation of the dust-emitting sediments from the Mojave Desert samples is similar to that of sediments described by González-Romero et al. (2023) for Moroccan samples, likely due to the presence of clays, Na salts, and precipitated carbonates. This aggregation inhibits aerodynamic entrainment, and dust emission should be primarily controlled by saltation bombardment (Shao et al., 1993). According to the XRD analysis, the occurrence of crystalline Fe oxides is limited to maghemite/magnetite in contrast to the hematite and goethite content found in Moroccan crusts (González-Romero et al., 2023). However, due to the low precision of the XRD for the detection of low contents of minerals such as hematite and goethite, their presence in the samples cannot be ruled out. In fact, both the EMIT standard products (Fig. 3) and the Fe mode of occurrence analysis discussed in the next section suggest the presence of hematite and goethite.

The EMIT standard products (Fig. 3) indicate the presence of phyllosilicates such as kaolinite, smectite, montmorillonite, and illite, broadly consistent with our results. Specifically, around Mesquite Lake, where elevated levels of gypsum and carbonates were detected, the EMIT results corroborate the significance of these minerals in the same vicinity. Similarly, in Coyote, Ivanpah, and Cronese lakes, there is agreement regarding the prevalence of illite and muscovite as the major clay minerals, alongside kaolinite. However, discrepancies arise in Soda Lake, where EMIT identifies a dominant presence of montmorillonite, contrasting with our XRD results indicating a predominance of illite, muscovite, and kaolinite. While Tetracorder identified montmorillonite as being predominant, illite, muscovite, and kaolinite could be on the order of 30% of the montmorillonite abundance and not show in the EMIT spectra without a more sophisticated non-linear radiative transfer model to find the relative abundances of these two minerals. This is due to the relative absorption strengths of the spectral features of these minerals

relative to those in montmorillonite. While our XRD analyses highlight the presence of maghemite/magnetite, these minerals do not present clear absorbing features in the spectral range of the EMIT instrument and are not considered within the 10 EMIT standard minerals. In contrast to the XRD results, EMIT highlights the significant presence of goethite in the northern sources (Mesquite and Ivanpah lakes). Conversely, in the southern sources (Soda, Cronese, and Coyote lakes), EMIT highlights a major mixture of Fe^{2+} and Fe^{3+} species. The limited precision of XRD for low proportions of Fe oxides underscores the need for complementary techniques and analyses to bolster our findings.

The mineralogical composition of the dry size-segregated fractions of the dust-emitting sediments is outlined in Table S4. The findings indicate that there is no significant size enrichment process in crusts; rather, there exists a relatively uniform distribution of quartz, feldspars, zeolites, and Fe oxides across all size fractions (Fig. 6). A slight, albeit not significant, enrichment of carbonates and clays is observed, along with a slight depletion of Na salts and gypsum in the finer fractions ($< 20 \mu\text{m}$). Additionally, pargasite shows a slight enrichment in the 40–80 μm fraction. In contrast, for aeolian ripples, quartz exhibits significant enrichment in the coarser fraction (250–500 μm) and depletion in the finer ones ($< 80 \mu\text{m}$). Regarding carbonates, clays, and Fe oxides, there is an enrichment towards the finer fractions ($< 20 \mu\text{m}$), while the content of feldspars remains relatively homogeneous. Pargasite content increases in the 40–80 μm fraction, and Na salts and gypsum are either not detected or present in trace amounts (Fig. 6). The notable disparity in the enrichment factor between crusts and aeolian ripples is partly attributed to the reduced amount of sand in crusts and the differing cohesion states: crusts exhibit high cohesion, resulting in a homogenized mineralogy across size fractions (as aggregates form a homogeneous concretion of minerals), while aeolian ripples display lower or negligible aggregation, leading to a slightly more heterogeneous mineralogy across size fractions compared to crusts.

3.3 Mode of occurrence of Fe

The average content of FeT in the crusts is $3.0 \pm 1.3 \text{ wt } \%$, while for aeolian ripples it is $1.9 \pm 1.1 \text{ wt } \%$. Among these crusts, $1.8 \pm 0.92 \text{ } \%$ of the FeT occurs as FeA, $17 \pm 7.2 \text{ } \%$ as FeD, $2.1 \pm 1.2 \text{ } \%$ as FeM, and $79 \pm 8.5 \text{ } \%$ as FeS (Tables 3 and S5). Aeolian ripples have very similar contents and modes of occurrence of Fe in the analysed samples of the Mojave Desert.

Among the crusts, Ivanpah has the highest FeT content at 4.9 %, followed by Cronese and Coyote lakes ($3.7 \pm 1.2 \text{ } \%$ and $3.5 \text{ } \%$, respectively), with Soda Lake showing a similar content ($3.1 \pm 1.2 \text{ } \%$). Mesquite has the lowest FeT ($1.6 \pm 0.53 \text{ } \%$), probably due to the dilution of detrital Fe-bearing minerals with salts and gypsum. FeS is the dominant mode of occurrence in most lakes, ranging from 68 % (one

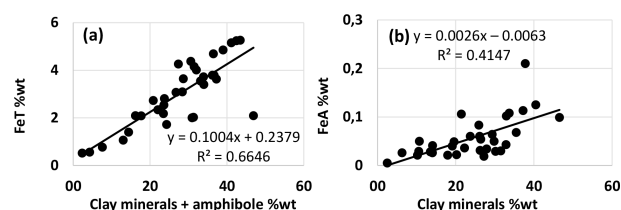


Figure 9. Cross-correlation plots of the clay contents and amphiboles with the FeT (a) and clay minerals and FeA (b), both in weight percent (wt %) of crusts.

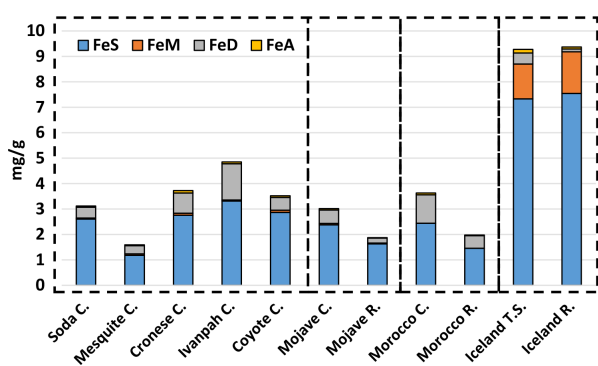
sample) at Ivanpah to $74 \pm 3.5 \text{ } \%$ and $74 \pm 13 \text{ } \%$ at Mesquite and Cronese and to $83 \pm 2.8 \text{ } \%$ and $82 \text{ } \%$ at Soda and Coyote lakes. The FeD is higher at Ivanpah ($29 \text{ } \%$), Cronese lakes ($21 \pm 11 \text{ } \%$), and Mesquite Lake ($20 \pm 2.7 \text{ } \%$) than at Soda and Coyote lakes ($14 \pm 2.5 \text{ } \%$ and $14 \text{ } \%$). FeM is higher at Mesquite Lake ($3.7 \pm 1.2 \text{ } \%$), followed by Cronese and Coyote lakes ($2.3 \pm 1.1 \text{ } \%$ and $2.4 \text{ } \%$) and Soda ($1.5 \pm 0.49 \text{ } \%$) and Ivanpah lakes ($0.82 \text{ } \%$). Finally, FeA is higher at Cronese Lake ($2.4 \pm 0.99 \text{ } \%$), compared to Coyote, Mesquite, Soda, and Ivanpah lakes ($1.8 \text{ } \%$, $1.8 \pm 0.93 \text{ } \%$, $1.5 \pm 0.81 \text{ } \%$, and $1.4 \text{ } \%$) (Tables 3 and S5). Crusts are enriched in FeT, FeD, and FeA compared to ripples, while ripples are enriched in FeM and FeS (Tables 3 and S5).

Overall, the bulk Fe content in crusts is driven by structural Fe from clays and amphiboles (as deduced from the high correlation shown in Fig. 9a), followed by small proportions of hematite and goethite (not detected by XRD), which are clearly higher at the northern lakes, Ivanpah and Mesquite (consistent with the highlighted presence of goethite in the EMIT standard products), probably due to the Precambrian and Cambrian metamorphic rocks that supply sediments. Furthermore, the easily exchangeable Fe is also driven by clay minerals (Fig. 9b).

Compared to crusts in other arid regions analysed by González-Romero et al. (2023, 2024), the analysed Mojave Desert crusts have similar FeT content to Moroccan crusts but are much lower than the Icelandic top sediments (loose surface sediments in Iceland according to González-Romero et al., 2024) ($3.0 \pm 1.3 \text{ } \%$, $3.6 \pm 0.71 \text{ } \%$, and $9.5 \pm 0.39 \text{ } \%$, for Mojave, Morocco, and Iceland, respectively). The proportion of FeS in FeT is similar to the Icelandic sediments but higher than in Moroccan samples ($79 \pm 8.5 \text{ } \%$ and $79 \pm 6.5 \text{ } \%$, and $67 \pm 2.4 \text{ } \%$, respectively). The proportion of FeM is clearly lower than that of Iceland but higher than that of Morocco ($2.1 \pm 1.2 \text{ } \%$ and $16 \pm 5.4 \text{ } \%$ for Mojave and Iceland; the Moroccan proportion is negligible). The FeD proportion is intermediate between Morocco and Iceland ($17 \pm 7.2 \text{ } \%$, $31 \pm 2.3 \text{ } \%$, and $3.5 \pm 1.5 \text{ } \%$, respectively), while the FeA proportion is similar to both Moroccan and Icelandic crusts ($1.8 \pm 0.92 \text{ } \%$, $1.3 \pm 0.39 \text{ } \%$, and $1.9 \pm 0.55 \text{ } \%$, respectively) (Fig. 10).

Table 3. Fe content in weight percent (wt %) for total Fe (FeT) content and in percent (%) for ascorbate Fe (FeA), dithionite (FeD), oxalate Fe (FeM), and structural Fe (FeS). NaN: not a number.

	FeT	FeA %	FeD %	FeM %	FeS %
Crusts	3.0 ± 1.3	1.8 ± 0.92	17 ± 7.2	2.1 ± 1.2	79 ± 8.5
Soda	3.1 ± 1.2	1.5 ± 0.81	14 ± 2.5	1.5 ± 0.49	83 ± 2.8
Cronese	3.7 ± 1.2	2.4 ± 0.99	21 ± 11	2.3 ± 1.1	74 ± 13
Coyote	3.5	1.8	14	2.4	82
Ivanpah	4.9	1.4	29	0.82	68
Mesquite	1.6 ± 0.53	1.8 ± 0.93	20 ± 2.7	3.7 ± 1.2	74 ± 3.5
Ripples	1.9 ± 1.1	1.4 ± 1.2	12 ± 5.6	2.4 ± 1.8	84 ± 7.5
Soda	2.0 ± 1.2	0.98 ± 0.39	10 ± 3.4	2.1 ± 1.8	87 ± 4.4
Cronese	2.3 ± 1.5	1.4 ± 0.35	14 ± 9.3	2.8 ± 2.9	82 ± 12
Coyote	1.3	3.4	26	3.0	68
Ivanpah	NaN	NaN	NaN	NaN	NaN
Mesquite	1.0 ± 1.1	3.6 ± 3.0	20 ± 1.2	4.4 ± 1.2	73 ± 4.1

**Figure 10.** Modes of occurrence of Fe comparison between the crusts' (C) playa lakes analysed in this study, the average of the crusts and ripples (R) in the Mojave Desert, Morocco, and the Icelandic top surface (TS). FeA refers to the exchangeable Fe and nano-sized Fe oxides, FeD is the Fe content in hematite and goethite, FeM is the Fe content in maghemite/magnetite, and FeS is the Fe content in Fe-bearing minerals.

4 Discussion and conclusions

The playa lakes sampled within the Mojave Desert can serve as significant dust-emitting sources in the region. Descriptions provided by Urban et al. (2018) and satellite imagery (Fig. 2) confirm the presence of desert dust emissions originated from these areas. The lithology, geological/tectonic evolution, and past and current climate conditions collectively contribute to the formation of these dust sources in the Mojave Desert.

Dust-emitting sediments in this region predominantly stem from substratum rocks, comprising mainly granitic and volcanic formations, along with metamorphic Pre-Cambrian, Cambrian, Paleozoic, and Mesozoic rocks. Endorheic basins, shaped by faulting during the Tertiary–Quaternary period,

accumulated fine sediments through erosion, transportation, and deposition processes. Wetter conditions prevailing during the Pleistocene epoch led to the formation of deep lakes within the basins, which gradually desiccated as the climate evolved. These arid conditions rendered the playa lakes susceptible to dust emission under specific atmospheric conditions. Notably, a particle size segregation is observed, transitioning from coarser sediments in the proximal alluvial areas towards finer particle crusts within the central regions of the lakes. In the playa lakes, finer sediments accumulate towards the centre of the lakes due to flood events inundating the central areas and ponding, which facilitates the deposition of coarser particles followed by top finer sediment sizes.

As represented in the conceptual model depicted in Fig. 11, the finer dust particle size distributions range from 8.4 to 99 μm inside Soda Lake and 46 to 111 μm outside Soda Lake, underscoring this sedimentation process. Comparisons with conceptual models proposed for other regions, such as those by González-Romero et al. (2023, 2024) for locations in Morocco and Iceland, reveal a similar transport fractionation phenomenon occurring in the Mojave Desert. These crusts, observed within Soda Lake, show enrichment in clay minerals, carbonate minerals, salts, and iron oxides, while experiencing depletion in coarser constituents such as feldspars and quartz.

In the Mojave Desert, there are two distinct types of playa lakes, characterized as wet and dry, depending on the regime of the groundwater table and its relationship with the surface, as described by Reynolds et al. (2007, 2009), Buck et al. (2011), Nield et al. (2016a, b), Urban et al. (2018), and Goudie (2018). Understanding the groundwater table regime is fundamental in this region due to its profound relation with the porosity of the crust and its consequential impact on mineralogy, including the precipitation and enrichment of salts (Fig. 11). This dynamic contrasts sharply with other concep-

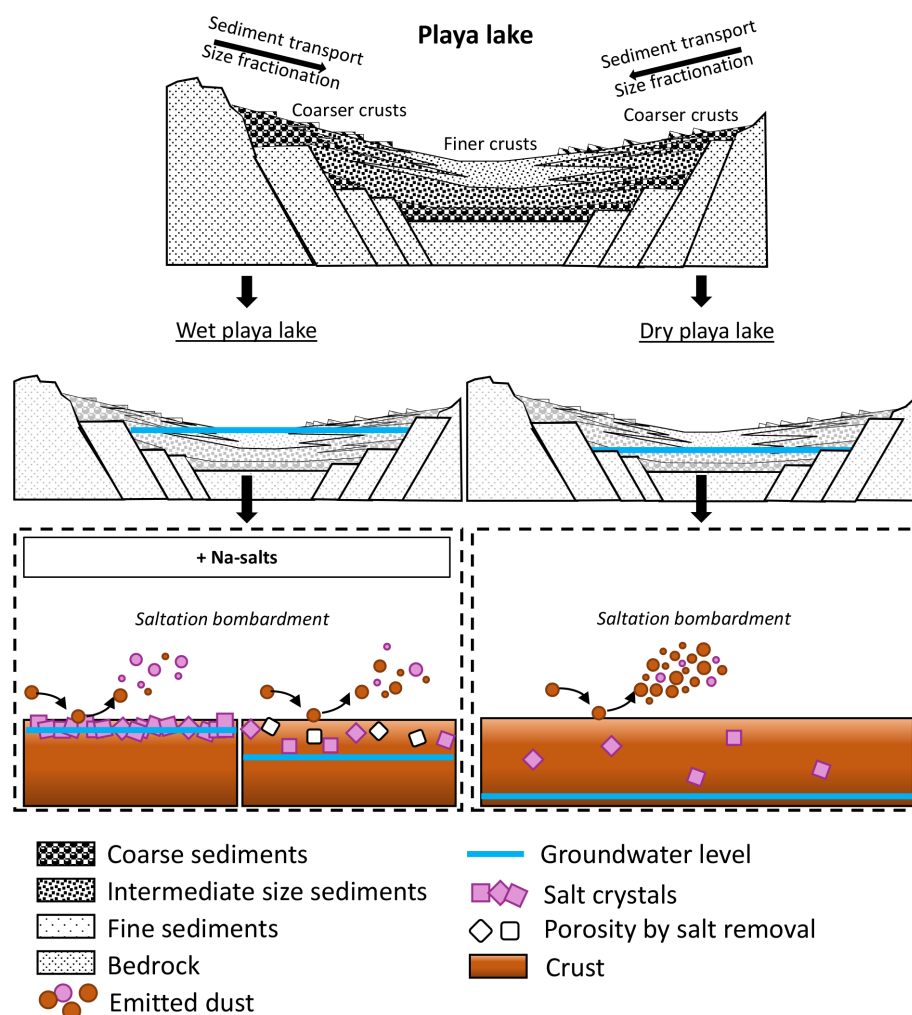


Figure 11. Conceptual model of wet and dry playa lake differences due to groundwater differences and how this can affect the mineralogy of the surface in the playa lakes. Also illustrated is the expected dust emission rate, major mineralogy, and modes of occurrence of Fe differences expected in the emitted dust.

tual models, where the relationship between crust formation and the groundwater table is either minimal or absent entirely. For instance, there is no or little relation between crusts and groundwater table in Morocco and in Iceland, where the water regime is largely influenced by flooding from glaciers (González-Romero et al., 2023, 2024). In wet playa lakes like Soda Lake, the presence of salty crusts, whether massive or spongy, is significantly pronounced. Conversely, in dry playa lakes such as Ivanpah, Coyote, and Cronese, the relationship of salt crusts is notably less prominent as the proportion of Na salts is lower (see Fig. 11).

At Soda Lake, a hard crust, measuring up to 0.5 m in thickness (Fig. 3), forms through the extensive precipitation of Na salts, particularly near the Zzyzx area, where a relatively constant mobilization of salts is due to the water table evaporation or vapour discharge from deeper parts of the sediment towards the surface (Nield et al., 2015, 2016a, b). Along the

edges of this massive crusty area, the frequent oscillation of the water table may result in the precipitation and dissolution of salts in lower quantities compared to the centre, leading to the formation of weaker crusts characterized by high porosity. These porous crusts may contribute to an increased dust emission rate compared to the hard salt crusts found in the centre. Dry lakes such as Ivanpah, Cronese, and Coyote do not exhibit the formation of spongy crusts due to the low concentrations of salts. In wet playas, strong dust emission may happen when very strong winds rip off thin crusts, exposing the fine-grained sediment beneath including lithogenic and salt mineral particles (Richard Reynolds, personal communication, 2024).

Particle aggregation facilitated by diagenetic salts and carbonate minerals is prevalent in the dust-emitting sediments sampled in the Mojave Desert, akin to the equivalent sediments found in the Moroccan Sahara. The average

Table 4. A summary of MDPSD (μm) and FDPSD (μm) median particle diameters, quartz (Qtz; wt %), feldspars (Feld.; wt %), clay mineral (Clay; wt %), carbonates (Carb.; wt %), Na salts (Na-S; wt %), gypsum (Gp; wt %), total Fe content (FeT; wt %), exchangeable Fe (FeA; wt %), dithionite Fe (FeD; wt %), oxalate Fe (FeM; wt %), and structural Fe (FeS; wt %) for Mojave and Moroccan crusts and Icelandic top sediments. NaN: not a number.

	MDPSD d(0.5)	FDPSD d(0.5)	Qtz	Feld.	Clay	Carb.	Na-S	Gp	FeT	FeA	FeD	FeM	FeS
Mojave Desert	92	37	16	37	24	6.6	7.3	3.1	3.0	0.06	0.53	0.06	2.4
Morocco	113	37	48	9.4	17	22	7.0	0.64	3.6	0.07	1.1	NaN	2.4
Iceland	55	56	0.21	20	NaN	NaN	NaN	NaN	9.3	0.15	0.43	1.4	7.3

grain size of the crusts from both regions is similar, with MDPSD values of $113 \pm 79 \mu\text{m}$ for Morocco and $92 \pm 74 \mu\text{m}$ for the Mojave Desert and FDPSD values of $37 \pm 77 \mu\text{m}$ and $37 \pm 48 \mu\text{m}$, respectively. These patterns contrast with the lower aggregation state and the finer MDPSD observed in Icelandic dust ($55 \pm 62 \mu\text{m}$) (Table 4).

In terms of mineralogy, crusts from the Mojave Desert are enriched in feldspars, clay minerals, Na salts, and gypsum, whereas crusts from the Moroccan Sahara are enriched in quartz and carbonates (Table 4). The mineralogy of Icelandic top sediments (loose surface sediments in Iceland according to González-Romero et al., 2024) differs due to their volcanic origin; however, both the Mojave Desert crusts and Icelandic top sediments contain similar amounts of zeolites. Salt enrichment in the crusts is primarily attributed to interactions with the groundwater table as shown in previous studies (Nield et al., 2016a, b; Urban et al., 2018; Goudie, 2018) (Fig. 11).

The total iron content (FeT) remains consistent throughout the samples collected in the Mojave Desert, with slightly higher levels observed in the Ivanpah crust, albeit diluted by the high salt content in the wet playa lake crusts or the elevated gypsum content in the Mesquite Lake. While the total Fe content is comparable between the Mojave Desert and Moroccan Sahara crusts (3.0 wt % and 3.6 wt %, respectively), it is substantially lower than in Icelandic top sediments (9.3 wt %). Exchangeable Fe proportions in FeT are similar among the three environments. The proportion of Fe from hematite and goethite in Mojave Desert crusts falls between that of Moroccan Sahara crusts and Icelandic top sediments (17 wt %, 31 wt %, and 0.5 wt %, respectively). The proportion of maghemite/magnetite in Mojave Desert crusts is much lower compared to Icelandic top sediments (2.1 % and 15 %, respectively). Finally, the proportion of structural Fe in the samples is similar across the three environments.

In conclusion, the dust-emitting sediments collected from the Mojave Desert exhibit distinct signatures in mineralogy and modes of occurrence of Fe compared to those from the Moroccan Sahara, despite similar particle sizes. These differences can influence emitted dust properties and associated impacts. Similarities in fully disturbed and minimally disturbed particle size distributions support comparable dust

emission mechanisms, with saltation bombardment playing a prominent role.

Code availability. The Tetracorder code used in this paper is provided at <https://github.com/PSI-edu/spectroscopy-tetracorder> by Clark (2023).

Data availability. Data used in this paper are given in the main paper itself and in the Supplement. If needed, data are also available upon request by emailing the authors.

Supplement. The supplement related to this article is available online at: <https://doi.org/10.5194/acp-24-9155-2024-supplement>.

Author contributions. Sample permits were obtained by BLE, RNG, and AMK. The samples were collected by CPGP, AGR, AMK, RNG, and XQ and analysed by AGR, MHC, and NM. EMIT mineralogy maps we produced by RG, PB, and RNC. PG provided the FoO map. AGR analysed the data and wrote of the original draft manuscript, supervised by CPGP and XQ. CPGP and XQ re-edited the manuscript and all authors contributed to data discussion, review, and paper finalization.

Competing interests. At least one of the (co-)authors is a member of the editorial board of *Atmospheric Chemistry and Physics*. The peer-review process was guided by an independent editor, and the authors also have no other competing interests to declare.

Disclaimer. Publisher's note: Copernicus Publications remains neutral with regard to jurisdictional claims made in the text, published maps, institutional affiliations, or any other geographical representation in this paper. While Copernicus Publications makes every effort to include appropriate place names, the final responsibility lies with the authors.

Acknowledgements. We thank Richard Reynolds and an anonymous reviewer for the helpful comments and suggestions to improve the manuscript.

The field campaign and its associated research, including this work, were funded by the European Research Council under the Horizon 2020 Research and Innovation programme through the ERC Consolidator Grant FRAGMENT (grant agreement no. 773051) and the AXA Research Fund through the AXA Chair on Sand and Dust Storms at BSC. Cristina González-Flórez was supported by a PhD fellowship from the Agència de Gestió d'Ajuts Universitaris i de Recerca (AGAUR) grant 2020_FI B 00678. Konrad Kandler was funded by the Deutsche Forschungsgemeinschaft (DFG, German Research Foundation, grant nos. 264907654 and 416816480). Martina Klose received funding through the Helmholtz Association's Initiative and Networking Fund (grant agreement no. VH-NG-1533). We acknowledge the EMIT project, which is supported by the NASA Earth Venture Instrument program, under the Earth Science Division of the Science Mission Directorate. We are grateful to Claire Blaske and Sahil Azad for assistance with sampling in the Mojave National Preserve. Samples within the preserve were collected under permit MOJA-2022-SCI-0034. We thank Rose Pettiette at the BLM office in Needles, CA, for advice and for allowing sampling on BLM land. We thank Jason Wallace and Anne Kelly from CSU Desert Studies Center at Zzyzx for their support during the campaign. Bethany L. Ehlmann, Rebecca N. Greenberger, and Abigail M. Keebler thank the Resnick Sustainability Institute at Caltech for partial support. Without all of the people mentioned, the sampling campaign would not have been successfully feasible.

Financial support. This research has been supported by the European Research Council, EU H2020 (Consolidator Grant FRAGMENT, grant no. 773051); the AXA Research Fund (AXA Chair on Sand and Dust Storms BSC); the Agència de Gestió d'Ajuts Universitaris i de Recerca (grant no. 2020_FI B 00678); the Deutsche Forschungsgemeinschaft (grant nos. 264907654 and 416816480); the Helmholtz Association (grant no. VH-NG-1533); and the Earth Sciences Division (NASA Earth Venture Instrument – Science Mission Directorate).

The article processing charges for this open-access publication were covered by the CSIC Open Access Publication Support Initiative through its Unit of Information Resources for Research (URICI).

Review statement. This paper was edited by Stelios Kazadzis and reviewed by Richard Reynolds and one anonymous referee.

References

Alfaro, S. C., Gaudichet, A., Gomes, L., and Maillé, M.: Modeling the size distribution of a soil aerosol produced by sandblasting, *J. Geophys. Res.-Atmos.*, 102, 11239–11249, 1997.

Atkinson, J. D., Murray, B. J., Woodhouse, M. T., Whale, T. F., Baustian, K. J., Carslaw, K. S., Dobbie, S., O'Sullivan, D., and Malkin, T. L.: The importance of feldspar for ice nucleation by mineral dust in mixed-phase clouds, *Nature*, 498, 355–358, 2013.

Baddock, M. C., Ginoux, P., Bullard, J. E., and Gill, T. E.: Do MODIS-defined dust sources have a geomorphological signature?, *Geophys. Res. Lett.*, 43, 2606–2613, 2016.

Baldo, C., Formenti, P., Nowak, S., Chevaillier, S., Cazaunau, M., Pangu, E., Di Biagio, C., Doussin, J.-F., Ignatyev, K., Dagsson-Waldhauserova, P., Arnalds, O., MacKenzie, A. R., and Shi, Z.: Distinct chemical and mineralogical composition of Icelandic dust compared to northern African and Asian dust, *Atmos. Chem. Phys.*, 20, 13521–13539, <https://doi.org/10.5194/acp-20-13521-2020>, 2020.

Bauer, S. E. and Koch, D.: Impact of heterogeneous sulfate formation at mineral dust surfaces on aerosol loads and radiative forcing in the Goddard Institute for Space Studies general circulation model, *J. Geophys. Res.-Atmos.*, 110, D17202, <https://doi.org/10.1029/2005JD005870>, 2005.

Buck, B. J., King, J., and Etyemezian, V.: Effects of salt mineralogy on dust emissions, Salton Sea, California, *Soil Sci. Soc. Am. J.*, 75, 1971–1985, 2011.

Bullard, J. E., Harrison, S. P., Baddock, M. C., Drake, N., Gill, T. E., McTainsh, G., and Sun, Y.: Preferential dust sources: A geomorphological classification designed for use in global dust-cycle models, *J. Geophys. Res.-Earth*, 116, F04034, <https://doi.org/10.1029/2011JF002061>, 2011.

Chatziparaschos, M., Daskalakis, N., Myriokefalitakis, S., Kalivitis, N., Nenes, A., Gonçalves Ageitos, M., Costa-Surós, M., Pérez García-Pando, C., Zanolli, M., Vrekoussis, M., and Kanakidou, M.: Role of K-feldspar and quartz in global ice nucleation by mineral dust in mixed-phase clouds, *Atmos. Chem. Phys.*, 23, 1785–1801, <https://doi.org/10.5194/acp-23-1785-2023>, 2023.

Cheary, R. W. and Coelho, A.: A fundamental parameters approach to X-ray line profile fitting, *J. Appl. Crystallogr.*, 25, 109–121, 1992.

Claquin, T., Schulz, M., and Balkanski, Y. J.: Modeling the mineralogy of atmospheric dust sources, *J. Geophys. Res.-Atmos.*, 104, 22243–22256, 1999.

Clark, R. N.: Tetracorder, GitHub [code], <https://github.com/PSI-edu/spectroscopy-tetracorder> (last access: 1 August 2024), 2023.

Clark, R. N.: PSI-edu/spectroscopy-tetracorder: Tetracorder 5.27 with expert systems to 5.27e + specpr, spectral libraries, and radiative transfer models (v5.27.0), Zenodo [code], <https://doi.org/10.5281/zenodo.11204505>, 2024.

Clark, R. N., Swayze, G. A., Livo, K. E., Brodrick, P., Noe Dobrea, E., Vijayarangan, S., Green, R. O., Wettergreen, D., Candela, A., Hendrix, A., Garcia-Pando, C. P., Pearson, N., Lane, M. D., Gonzalez-Romero, A., Querol, X., the EMIT team, and TREX team: Imaging spectroscopy: Earth and planetary remote sensing with the PSI Tetracorder and expert systems: from Rovers to EMIT and Beyond, *Planetary Science Journal*, in press, 2024.

Crumevolle, S., Gomes, L., Tulet, P., Matsuki, A., Schwarzenboeck, A., and Crahan, K.: Increase of the aerosol hygroscopicity by cloud processing in a mesoscale convective system: a case study from the AMMA campaign, *Atmos. Chem. Phys.*, 8, 6907–6924, <https://doi.org/10.5194/acp-8-6907-2008>, 2008.

De la Torre, A. G., Bruque, S., and Aranda, M. A. G.: Rietveld quantitative amorphous content analysis, *J. Appl. Crystallogr.*, 34, 196–202, 2001.

De Longueville, F., Hountondji, Y. C., Henry, S., and Ozer, P.: What do we know about effects of desert dust on air quality and human

- health in West Africa compared to other regions?, *Sci. Total Environ.*, 409, 1–8, 2010.
- Dibblee, T. W.: Areal geology of the western Mojave Desert California, Geological Survey Professional Paper 522, <https://doi.org/10.3133/pp522>, 1967.
- Di Biagio, C., Formenti, P., Balkanski, Y., Caponi, L., Cazaunau, M., Pangui, E., Journet, E., Nowak, S., Andreae, M. O., Kandler, K., Saeed, T., Piketh, S., Seibert, D., Williams, E., and Doussin, J.-F.: Complex refractive indices and single-scattering albedo of global dust aerosols in the shortwave spectrum and relationship to size and iron content, *Atmos. Chem. Phys.*, 19, 15503–15531, <https://doi.org/10.5194/acp-19-15503-2019>, 2019.
- Eghbal, M. K. and Southard, R. J.: Mineralogy of Aridisols on Dissected Alluvial Fans, Western Mojave Desert, California, *Soil Sci. Soc. Am. J.*, 57, 538–544, 1993.
- Engelbrecht, J. P., Moosmüller, H., Pincock, S., Jayanty, R. K. M., Lersch, T., and Casuccio, G.: Technical note: Mineralogical, chemical, morphological, and optical interrelationships of mineral dust re-suspensions, *Atmos. Chem. Phys.*, 16, 10809–10830, <https://doi.org/10.5194/acp-16-10809-2016>, 2016.
- Floyd, K. W., and Gill, T. E.: The association of land cover with aeolian sediment production at Jornada Basin, New Mexico, USA, *Aeolian Res.*, 3, 55–66, 2011.
- Formenti, P., Caqueneau, S., Chevaillier, S., Klaver, A., Desboeufs, K., Rajot, J. L., Belin, S., and Briois, V.: Dominance of goethite over hematite in iron oxides of mineral dust from Western Africa: Quantitative partitioning by X-ray absorption spectroscopy, *J. Geophys. Res.-Atmos.*, 119, 12740–12754, <https://doi.org/10.1002/2014jd021668>, 2014.
- Frank, T. D., Di Girolamo, L., and Geegan, S.: The spatial and temporal variability of aerosol optical depths in the Mojave desert of southern California, *Remote Sens. Environ.*, 107, 54–64, <https://doi.org/10.1016/j.rse.2006.06.024>, 2007.
- Ginoux, P., Chin, M., Tegen, I., Prospero, J. M., Holben, B., Dubovik, O., and Lin, S. J.: Sources and distributions of dust aerosols simulated with the GOCART model, *J. Geophys. Res.-Atmos.*, 106, 20255–20273, 2001.
- Ginoux, P., Prospero, J. M., Gill, T. E., Hsu, N. C., and Zhao, M.: Global-scale attribution of anthropogenic and natural dust sources and their emission rates based on MODIS Deep Blue aerosol products, *Rev. Geophys.*, 50, RG3005, <https://doi.org/10.1029/2012RG000388>, 2012.
- Goldstein, H. L., Breit, G. N., and Reynolds, R. L.: Controls on the chemical composition of saline surface crusts and emitted dust from a wet playa in the Mojave Desert (USA), *J. Arid Environ.*, 140, 50–66, 2017.
- González-Flórez, C., Klose, M., Alastuey, A., Dupont, S., Escribano, J., Etyemezian, V., Gonzalez-Romero, A., Huang, Y., Kandler, K., Nikolich, G., Panta, A., Querol, X., Reche, C., Yus-Díez, J., and Pérez García-Pando, C.: Insights into the size-resolved dust emission from field measurements in the Moroccan Sahara, *Atmos. Chem. Phys.*, 23, 7177–7212, <https://doi.org/10.5194/acp-23-7177-2023>, 2023.
- González-Romero, A., González-Flórez, C., Panta, A., Yus-Díez, J., Reche, C., Córdoba, P., Moreno, N., Alastuey, A., Kandler, K., Klose, M., Baldo, C., Clark, R. N., Shi, Z., Querol, X., and Pérez García-Pando, C.: Variability in sediment particle size, mineralogy, and Fe mode of occurrence across dust-source inland drainage basins: the case of the lower Drâa Valley, Morocco, *Atmos. Chem. Phys.*, 23, 15815–15834, <https://doi.org/10.5194/acp-23-15815-2023>, 2023.
- González-Romero, A., González-Flórez, C., Panta, A., Yus-Díez, J., Córdoba, P., Alastuey, A., Moreno, N., Kandler, K., Klose, M., Clark, R. N., Ehlmann, B. L., Greenberger, R. N., Keebler, A. M., Brodrick, P., Green, R. O., Querol, X., and Pérez García-Pando, C.: Probing Iceland's dust-emitting sediments: particle size distribution, mineralogy, cohesion, Fe mode of occurrence, and reflectance spectra signatures, *Atmos. Chem. Phys.*, 24, 6883–6910, <https://doi.org/10.5194/acp-24-6883-2024>, 2024.
- Goudie, A.: Dust storms and ephemeral lakes, *Desert*, 23, 153–164, 2018.
- Goudie, A. S. and Middleton, N. J.: *Desert dust in the global system*, Springer, Heidelberg, ISBN 978-3-540-32355-6, 288 pp., 2006.
- Green, R. O., Mahowald, N., Ung, C., Thompson, D. R., Bator, L., Bennet, M., and Zan, J.: The earth surface mineral dust source investigation: an earth science imaging spectroscopy mission, in: *IEEE Aerospace Conference*, Big Sky, MT, USA, 7–14 March 2020, IEEE, <https://doi.org/10.1109/AERO47225.2020.9172731>, 2020.
- Harrison, A. D., Lever, K., Sanchez-Marroquin, A., Holden, M. A., Whale, T. F., Tarn, M. D., McQuaid, J. B., and Murray, B. J.: The ice-nucleating ability of quartz immersed in water and its atmospheric importance compared to K-feldspar, *Atmos. Chem. Phys.*, 19, 11343–11361, <https://doi.org/10.5194/acp-19-11343-2019>, 2019.
- Hettiarachchi, E., Reynolds, R. L., Goldstein, H. L., Moskowitz, B., and Rubasinghe, G.: Bioavailable iron production in airborne mineral dust: Controls by chemical composition and solar flux, *Atmos. Environ.*, 205, 90–102, 2019.
- Hettiarachchi, E., Ivanov, S., Kieft, T., Goldstein, H. L., Moskowitz, B. M., Reynolds, R. L., and Rubasinghe, G.: Atmospheric processing of iron-bearing mineral dust aerosol and its effect on growth of a marine diatom, *Cyclotella meneghiniana*, *Environ. Sci. Technol.*, 55, 871–881, 2020.
- Honke, J. S., Pigati, J. S., Wilson, J., Bright, J., Goldstein, H. L., Skipp, G. L., Reheis, M. C., and Havens, J. C.: Late Quaternary paleohydrology of desert wetlands and pluvial lakes in the Soda Lake basin, central Mojave Desert, California (USA), *Quaternary Sci. Rev.*, 216, 89–106, <https://doi.org/10.1016/j.quascirev.2019.05.021>, 2019.
- Ibáñez, J., Font, O., Moreno, N., Elvira, J. J., Alvarez, S., and Querol, X.: Quantitative Rietveld analysis of the crystalline and amorphous phases in coal fly ashes, *Fuel*, 105, 314–317, 2013.
- Jennings, C. W., Burnett, J. L., and Troxel, B. W.: *Geologic map of California: Trona sheet*, Geologic Atlas of California, GAM-23, 1:250,000, California Division of Mines and Geology, https://www.davidrumsey.com/luna/servlet/detail/RUMSEY~8~1~324984~90094045:Geologic-Map-of-California%2C-Trona-S?sort=Pub_List_No_InitialSort%2CPub_Date%2CPub_List_No%2CSeries_No&qvq=q:trona%20sheet;sort:Pub_List_No_InitialSort%2CPub_Date%2CPub_List_No%2CSeries_No;lc:RUMSEY~8~1&mi=3&trs=4 (last access: 1 August 2024), 1962.
- Jickells, T. D., An, Z. S., Andersen, K. K., Baker, A. R., Bergametti, G., Brooks, N., Cao, J. J., Boyd, P. W., Duce, R. A., Hunter, K. A., Kawahata, H., Kubilay, N., laRoche, J., Liss, P. S., Mahowald, N., Prospero, J. M., Ridgwell, A. J., Tegen, I., and Torres, R.:

- Global iron connections between desert dust, ocean biogeochemistry, and climate, *Science*, 308, 67–71, 2005.
- Journet, E., Balkanski, Y., and Harrison, S. P.: A new data set of soil mineralogy for dust-cycle modeling, *Atmos. Chem. Phys.*, 14, 3801–3816, <https://doi.org/10.5194/acp-14-3801-2014>, 2014.
- Karanasiou, A., Moreno, N., Moreno, T., Viana, M., de Leeuw, F., and Querol, X.: Health effects from Sahara dust episodes in Europe: Literature review and research gaps, *Environ. Int.*, 47, 107–114, 2012.
- Kok, J. F., Adebisi, A. A., Albani, S., Balkanski, Y., Checa-Garcia, R., Chin, M., Colarco, P. R., Hamilton, D. S., Huang, Y., Ito, A., Klose, M., Li, L., Mahowald, N. M., Miller, R. L., Obiso, V., Pérez García-Pando, C., Rocha-Lima, A., and Wan, J. S.: Contribution of the world's main dust source regions to the global cycle of desert dust, *Atmos. Chem. Phys.*, 21, 8169–8193, <https://doi.org/10.5194/acp-21-8169-2021>, 2021.
- Li, L., Mahowald, N. M., Miller, R. L., Pérez García-Pando, C., Klose, M., Hamilton, D. S., Gonçalves Ageitos, M., Ginoux, P., Balkanski, Y., Green, R. O., Kalashnikova, O., Kok, J. F., Obiso, V., Paynter, D., and Thompson, D. R.: Quantifying the range of the dust direct radiative effect due to source mineralogy uncertainty, *Atmos. Chem. Phys.*, 21, 3973–4005, <https://doi.org/10.5194/acp-21-3973-2021>, 2021.
- Machiels, L., Mertens, G., and Elsen, J.: Rietveld Refinement strategy for Quantitative Phase analysis of Partially Amorphous zeolitized tuffaceous, *Geol. Belg.*, 13, 183–196, 2010.
- Madsen, I. C., Scarlett, N. V. Y., Cranswick, L. M. D., and Lwin, T.: Outcomes of the international union of crystallography commission on powder diffraction round robin on quantitative phase analysis: Samples 1a to 1h, *J. Appl. Crystallogr.*, 34, 409–426, 2001.
- Miller, D. M., Menges, C. M., and Lidke, D. J.: Generalized surficial geologic map of the Fort Irwin area, San Bernardino County, California, 1 : 100,000, U. S. Geological Survey, Open-File Report OF-2013-1024-B, <https://doi.org/10.3133/ofr20131024B>, 2014.
- Miller, D. M., Dudash, S. L., and McGeehin, J. P.: Paleoclimate record for Lake Coyote, California, and the Last Glacial Maximum and deglacial paleohydrology (25 to 14 cal ka) of the Mojave River, in: *From Saline to Freshwater: The Diversity of Western Lakes in Space and Time*, edited by: Starratt, S. W. and Rosen, M. R., Geological Society of America Special Paper 536, 1–20, [https://doi.org/10.1130/2018.2536\(12\)](https://doi.org/10.1130/2018.2536(12)), 2018.
- Nield, J. M., Bryant, R. G., Wiggs, G. F., King, J., Thomas, D. S., Eckardt, F. D., and Washington, R.: The dynamism of salt crust patterns on playas, *Geology*, 43, 31–34, 2015.
- Nield, J. M., Neuman, C. M., O'Brien, P., Bryant, R. G., and Wiggs, G. F.: Evaporative sodium salt crust development and its wind tunnel derived transport dynamics under variable climatic conditions, *Aeolian Res.*, 23, 51–62, 2016a.
- Nield, J. M., Wiggs, G. F., King, J., Bryant, R. G., Eckardt, F. D., Thomas, D. S., and Washington, R.: Climate–surface–pore-water interactions on a salt crusted playa: implications for crust pattern and surface roughness development measured using terrestrial laser scanning, *Earth Surf. Proc. Land.*, 41, 738–753, 2016b.
- Obiso, V., Gonçalves Ageitos, M., Pérez García-Pando, C., Perlwitz, J. P., Schuster, G. L., Bauer, S. E., Di Biagio, C., Formenti, P., Tsigaridis, K., and Miller, R. L.: Observationally constrained regional variations of shortwave absorption by iron oxides emphasize the cooling effect of dust, *Atmos. Chem. Phys.*, 24, 5337–5367, <https://doi.org/10.5194/acp-24-5337-2024>, 2024.
- Panta, A., Kandler, K., Alastuey, A., González-Flórez, C., González-Romero, A., Klose, M., Querol, X., Reche, C., Yus-Díez, J., and Pérez García-Pando, C.: Insights into the single-particle composition, size, mixing state, and aspect ratio of freshly emitted mineral dust from field measurements in the Moroccan Sahara using electron microscopy, *Atmos. Chem. Phys.*, 23, 3861–3885, <https://doi.org/10.5194/acp-23-3861-2023>, 2023.
- Paulot, F., Ginoux, P., Cooke, W. F., Donner, L. J., Fan, S., Lin, M.-Y., Mao, J., Naik, V., and Horowitz, L. W.: Sensitivity of nitrate aerosols to ammonia emissions and to nitrate chemistry: implications for present and future nitrate optical depth, *Atmos. Chem. Phys.*, 16, 1459–1477, <https://doi.org/10.5194/acp-16-1459-2016>, 2016.
- Pérez, C., Nickovic, S., Pejanovic, G., Baldasano, J. M., and Özsoy, E.: Interactive dust-radiation modeling: A step to improve weather forecasts, *J. Geophys. Res.-Atmos.*, 111, D16206, <https://doi.org/10.1029/2005JD006717>, 2006.
- Pérez García-Pando, C., Stanton, M. C., Diggle, P. J., Trzaska, S., Miller, R. L., Perlwitz, J. P., Baldasano, J. M., Cuevas, E., Ceccato, P., Yaka, P., and Thomson, M. C.: Soil dust aerosols and wind as predictors of seasonal meningitis incidence in Niger, *Environ. Health Persp.*, 122, 679–686, 2014.
- Perlwitz, J. P., Pérez García-Pando, C., and Miller, R. L.: Predicting the mineral composition of dust aerosols – Part 1: Representing key processes, *Atmos. Chem. Phys.*, 15, 11593–11627, <https://doi.org/10.5194/acp-15-11593-2015>, 2015.
- Potter, C. and Coppernoll-Houston, D.: Controls on land surface temperature in deserts of southern California derived from MODIS satellite time series analysis, 2000 to 2018, *Climate*, 7, 32, <https://doi.org/10.3390/cli7020032>, 2019.
- Querol, X.: The Occurrence and Distribution of Trace Elements in the Teruel Mining District Coals and their Behaviour during Coal Combustion, European Coal and Steel Community Project 7220/ED/014, 1993.
- Querol, X., Whateley, M. K. G., Fernandez-Turiel, J. L., and Tunçali, E.: Geological controls on the mineralogy and geochemistry of the Bepazari lignite, Central Anatolia, Turkey, *Int. J. Coal Geol.*, 33, 255–271, 1997.
- Reheis, M. C.: Dust deposition downwind of Owens (dry) Lake, 1991–1994: Preliminary findings, *J. Geophys. Res.-Atmos.*, 102, 25999–26008, 1997.
- Reheis, M. C. and Kihl, R.: Dust deposition in southern Nevada and California, 1984–1989: Relations to climate, source area, and source lithology, *J. Geophys. Res.-Atmos.*, 100, 8893–8918, 1995.
- Reheis, M. C., Goodmacher, J. C., Harden, J. W., McFadden, L. D., Rockwell, T. K., Shroba, R. R., Sowers, J. M., and Taylor, E. M.: Quaternary soils and dust deposition in southern Nevada and California, *Geol. Soc. Am. Bull.*, 107, 1003–1022, 1995.
- Reheis, M. C., Budahn, J. R., Lamothe, P. J., and Reynolds, R. L.: Compositions of modern dust and surface sediments in the Desert Southwest, United States, *J. Geophys. Res.-Earth*, 114, F01028, <https://doi.org/10.1029/2008JF001009>, 2009.
- Reheis, M. C., Bright, J., Lund, S. P., Miller, D. M., Skipp, G., and Fleck, R. J.: A half-million-year record of paleoclimate from

- the Lake Manix core, Mojave Desert, California, *Palaeogeogr. Palaeoclimatol.*, 365–366, 11–37, 2012.
- Reynolds, R. L., Reheis, M., Yount, J., and Lamothe, P.: Composition of aeolian dust in natural traps on isolated surfaces of the central Mojave Desert – Insights to mixing, sources, and nutrient inputs, *J. Arid Environ.*, 66, 42–61, 2006.
- Reynolds, R. L., Yount, J. C., Reheis, M., Goldstein, H., Chavez Jr., P., Fulton, R., Whitney, J., Fuller, C., and Forester, R. M.: Dust emission from wet and dry playas in the Mojave Desert, USA, *Earth Surf. Proc. Land.*, 32, 1811–1827, 2007.
- Reynolds, R. L., Bogle, R., Vogel, J., Goldstein, H., and Yount, J.: Dust emission at Franklin Lake Playa, Mojave Desert (USA): Response to meteorological and hydrologic changes 2005–2008, *Nat. Resour. Env. Iss.*, 15, 105–116, 2009.
- Rietveld, H. M.: A profile refinement method for nuclear and magnetic structures, *J. Appl. Crystallogr.* 2, 65–71, 1969.
- Scanza, R. A., Mahowald, N., Ghan, S., Zender, C. S., Kok, J. F., Liu, X., Zhang, Y., and Albani, S.: Modeling dust as component minerals in the Community Atmosphere Model: development of framework and impact on radiative forcing, *Atmos. Chem. Phys.*, 15, 537–561, <https://doi.org/10.5194/acp-15-537-2015>, 2015.
- Scarlett, N. and Madsen, I.: Quantification of phases with partial or no known crystal structures, *Powder Diffr.*, 21, 278–284, 2006.
- Shao, Y.: A model for mineral dust emission, *J. Geophys. Res.-Atmos.*, 106, 20239–20254, 2001.
- Shao, Y., Raupach, M. R., and Findlater, P. A.: Effect of saltation bombardment on the entrainment of dust by wind, *J. Geophys. Res.-Atmos.*, 98, 12719–12726, 1993.
- Shao, Y., Wyrwoll, K. H., Chappell, A., Huang, J., Lin, Z., McTainsh, G. H., Mikami, M., Tanaka, T. Y., Wang, X., and Yoon, S.: Dust cycle: An emerging core theme in Earth system science, *Aeolian Res.*, 2, 181–204, 2011.
- Shi, Z. B., Krom, M. D., and Bonneville, S.: Formation of Iron Nanoparticles and Increase in Iron Reactivity in Mineral Dust during Simulated Cloud Processing, *Environ. Sci. Technol.* 43, 6592–6596, 2009.
- Sperazza, M., Moore, J. N., and Hendrix, M.: High-Resolution particle size analysis of naturally occurring very fine-grained sediment through laser diffractometry, *J. Sediment. Res.*, 74, 736–743, 2004.
- Stout, J. E. and Lee, J. A.: Indirect evidence of wind erosion trends on the Southern High Plains of North America, *J. Arid Environ.*, 55, 43–61, 2003.
- Sullivan, R. C., Guazzotti, S. A., Sodeman, D. A., Tang, Y., Carmichael, G. R., and Prather, K. A.: Mineral dust is a sink for chlorine in the marine boundary layer, *Atmos. Environ.*, 41, 7166–7179, 2007.
- Thorez, J.: Practical Identification of Clay Minerals: A Handbook for Teachers and Students in Clay Mineralogy, Institute of mineralogy, Liège State University, Belgium, Lelotte, 90 pp., 1976.
- Tong, D. Q., Dan, M., Wang, T., and Lee, P.: Long-term dust climatology in the western United States reconstructed from routine aerosol ground monitoring, *Atmos. Chem. Phys.*, 12, 5189–5205, <https://doi.org/10.5194/acp-12-5189-2012>, 2012.
- TOPAS: TOPAS and TOPAS-Academic: an optimization program integrating computer algebra and crystallographic objects written in C++, *J. Appl. Crystallogr.*, 51, 210–218, 2018.
- Urban, F. E., Reynolds, R. L., and Fulton, R.: The dynamic interaction of climate, vegetation, and dust emission, Mojave Desert, USA, in: *Arid Environments and Wind Erosion*, edited by: Fernandez-Bernal, A. and De La Rosa, M. A., NOVA Science Publishers, Inc., 243–267, ISBN 978-1-60692-411-2, 2009.
- Urban, F. E., Goldstein, H. L., Fulton, R., and Reynolds, R. L.: Unseen dust emission and global dust abundance: documenting dust emission from the Mojave Desert (USA) by daily remote camera imagery and wind-erosion measurements, *J. Geophys. Res.-Atmos.*, 123, 8735–8753, 2018.
- USGS: U. S. Geological Survey Open-File Report 01-041, A Laboratory Manual for X-Ray Powder Diffraction, <https://pubs.usgs.gov/of/2001/of01-041/htmldocs/methods/oamount.htm>, last access: 17 January 2024.
- Vandenberghe, R. E., Barrero, C. A., Da Costa, G. M., Van San, E., and De Grave, E.: Mössbauer characterization of iron oxides and (oxy) hydroxides: the present state of the art, *Hyperfine Interact.*, 126, 247–259, 2000.
- Weaver, C., Ginoux, P., Hsu, N., Chou, M.-D., and Joiner, J.: Radiative forcing of Saharan dust: GOCART model simulations compared with ERBE data, *J. Atmos. Sci.*, 59, 736–747, 2002.
- Whitney, J. W., Breit, G. N., Buckingham, S. E., Reynolds, R. L., Bogle, R. C., Luo, L., Goldstein, H. L., and Vogel, J. M.: Aeolian responses to climate variability during the past century on Mesquite Lake Playa, Mojave Desert, *Geomorphology*, 230, 13–25, 2015.
- Young, R. A.: *The Rietveld method*. International Union of Crystallography, Oxford University Press, UK, 1993.
- Zubko, N., Munoz, O., Zubko, E., Gritsevich, M., Escobar-Cerezo, J., Berg, M. J., and Peltoniemi, J.: Light scattering from volcanic-sand particles in deposited and aerosol form, *Atmos. Environ.*, 215, 116813, <https://doi.org/10.1016/j.atmosenv.2019.06.051>, 2019.